










An optimized genetically encoded dual reporter for simultaneous ratio imaging of Ca²⁺ and H⁺ reveals new insights into ion signaling in plants

Kunkun Li¹ , Juan Prada² , Daniel S. C. Damineli^{3,4} , Anja Liese⁵ , Tina Romeis⁵ , Thomas Dandekar² , José A. Feijó³ , Rainer Hedrich¹  and Kai Robert Konrad¹ 

¹Department of Botany I, Julius-Von-Sachs Institute for Biosciences, University of Wuerzburg, Wuerzburg 97082, Germany; ²Department of Bioinformatics, University of Wuerzburg, Wuerzburg 97074, Germany; ³Department of Cell Biology & Molecular Genetics, University of Maryland, 2136 Bioscience Research Bldg, College Park, MD 20742-5815, USA; ⁴Department of Pediatrics, Faculdade de Medicina da Universidade de São Paulo, São Paulo, SP 01246-903, Brazil; ⁵Leibniz Institute of Plant Biochemistry, Halle (Saale) 06120, Germany

Summary

Author for correspondence:
Kai Robert Konrad
Email: kai.konrad@botanik.uni-wuerzburg.de

Received: 29 September 2020
Accepted: 23 December 2020

New Phytologist (2021) 230: 2292–2310
doi: 10.1111/nph.17202

Key words: abscisic acid (ABA), calcium, flg22, guard cells, imaging, ion signaling, pH, pollen tube.

- Whereas the role of calcium ions (Ca²⁺) in plant signaling is well studied, the physiological significance of pH-changes remains largely undefined.
- Here we developed CapHensor, an optimized dual-reporter for simultaneous Ca²⁺ and pH ratio-imaging and studied signaling events in pollen tubes (PTs), guard cells (GCs), and mesophyll cells (MCs). Monitoring spatio-temporal relationships between membrane voltage, Ca²⁺- and pH-dynamics revealed interconnections previously not described.
- In tobacco PTs, we demonstrated Ca²⁺-dynamics lag behind pH-dynamics during oscillatory growth, and pH correlates more with growth than Ca²⁺. In GCs, we demonstrated abscisic acid (ABA) to initiate stomatal closure via rapid cytosolic alkalization followed by Ca²⁺ elevation. Preventing the alkalization blocked GC ABA-responses and even opened stomata in the presence of ABA, disclosing an important pH-dependent GC signaling node. In MCs, a flg22-induced membrane depolarization preceded Ca²⁺-increases and cytosolic acidification by c. 2 min, suggesting a Ca²⁺/pH-independent early pathogen signaling step. Imaging Ca²⁺ and pH resolved similar cytosol and nuclear signals and demonstrated flg22, but not ABA and hydrogen peroxide to initiate rapid membrane voltage-, Ca²⁺- and pH-responses.
- We propose close interrelation in Ca²⁺- and pH-signaling that is cell type- and stimulus-specific and the pH having crucial roles in regulating PT growth and stomata movement.

Introduction

Plant growth, development and adaptation are influenced by biotic and abiotic stimuli that must be perceived and transduced to elicit physiological responses. The role of calcium ions (Ca²⁺) as a second messenger has been studied intensively, but the role of protons (H⁺/pH) as a signaling mechanism has proved more recalcitrant to understand. Ca²⁺ and H⁺ can function as second messengers in many stress responses, such as pathogen- and drought-stress (Gao *et al.*, 2004; Kudla *et al.*, 2010; Reddy *et al.*, 2011; Romeis & Herde, 2014; Wilkins *et al.*, 2016). Changes in free cytosolic Ca²⁺-concentration ([Ca²⁺]_{cyt}) and free cytosolic H⁺-concentration ([H⁺]_{cyt}) and membrane voltage (V_m) are associated with early electric signaling (Felle *et al.*, 2005; Mousavi *et al.*, 2013; Choi *et al.*, 2017; Vincent *et al.*, 2017; Devireddy *et al.*, 2018; Kumari *et al.*, 2019). However, the hierarchy and possible interdependence of these three signaling components remain an intriguing fundamental question.

Guard cells (GCs) and pollen tubes (PTs) are the best studied plant cell types in terms of Ca²⁺-, pH- and ion-signaling (Murata

et al., 2015; Jezek & Blatt, 2017; Michard *et al.*, 2017; Konrad *et al.*, 2018). The mechanisms by which the phytohormone abscisic acid (ABA) and pathogen attack lead to stomatal closure has been studied intensively during the last decades (Kollist *et al.*, 2014; McLachlan *et al.*, 2014; Murata *et al.*, 2015; Chen *et al.*, 2020). Perception of the bacterial flagella epitope flg22 (Melotto *et al.*, 2006) and ABA seem to share common [Ca²⁺]_{cyt} downstream signaling networks (McLachlan *et al.*, 2014; Güzel Deger *et al.*, 2015; Zheng *et al.*, 2018). A mechanism similarly to GCs is thought to operate also in mesophyll cells (MCs) (Montillet *et al.*, 2013; Güzel Deger *et al.*, 2015) albeit it can be triggered by other stimuli (Elzenga *et al.*, 1995; Elzenga & Volkenburgh, 1997; Stoelzle *et al.*, 2003; Roelfsema *et al.*, 2012). Genetic evidence support the concept that Ca²⁺-dependent responses branched from the ABA pathway in GCs, yet in mesophyll pathogen-induced signaling, the Ca²⁺-dependent protein kinases (CDPKs) were likely co-opted to activate Ca²⁺-channels through reactive oxygen species (ROS) generated by NADPH-oxidases (Mori *et al.*, 2006; Boudsocq & Sheen, 2013; Merilo *et al.*, 2013; Brandt *et al.*, 2015; Yuan *et al.*, 2017; Tian *et al.*, 2019). CDPKs and ROS-signaling were

shown to be involved in immunity and ABA signaling in both GCs and MCs (Boudsocq & Sheen, 2013; Suzuki *et al.*, 2013; Kadota *et al.*, 2014; Sierla *et al.*, 2016) but are not associated with early electric response and the initiation of stomatal closure (Güzel Deger *et al.*, 2015). It should be noted that GCs need to integrate various signals from antagonistic stimuli, many of which use Ca^{2+} as a second messenger. Stomatal opening was reported to be associated with an increase in $[\text{Ca}^{2+}]_{\text{cyt}}$ (Irving *et al.*, 1992; Cousson & Vavasseur, 1998; Young *et al.*, 2006; Harada & Shimazaki, 2008) along with a cytosolic acidification in GCs, whereas ABA-induced stomatal closure was associated with a similar $[\text{Ca}^{2+}]_{\text{cyt}}$ rise but cytosolic alkalization (Irving *et al.*, 1992). This raises questions about the specificity of $[\text{Ca}^{2+}]_{\text{cyt}}$ -changes in stoma behavior and implies $[\text{H}^+]_{\text{cyt}}$ -changes as an important signal transmitter. Changes in extracellular H^+ -fluxes as well as $[\text{H}^+]_{\text{cyt}}$ -dynamics are coupled to pathogen and ABA-triggered stomatal closure in GCs (Irving *et al.*, 1992; Yan *et al.*, 2015) and are associated with early defense responses in the mesophyll (Jeworutzki *et al.*, 2010). However, the physiological role of pH-changes in all these responses is still unclear and reports on temporal aspects of pH signaling are rare. A cytosolic alkalization in GCs begins *c.* 2 min after ABA exposure (Irving *et al.*, 1992; Blatt & Armstrong, 1993) and precedes ROS production during stomatal closure (Suhita *et al.*, 2004; Ma *et al.*, 2013). Early responses in MCs upon perception of flg22 include an apoplastic alkalization (Kimura *et al.*, 2017) as well as ROS-production and Ca^{2+} -influx via NADPH oxidases and cyclic nucleotide-gated channels (CNGCs) or glutamate receptor-like channels (GLRs), respectively (McLachlan *et al.*, 2014; Moeder *et al.*, 2019; Tian *et al.*, 2019).

An interweaving, but still not totally understood $[\text{Ca}^{2+}]_{\text{cyt}}$ and $[\text{H}^+]_{\text{cyt}}$ signaling network exists in PTs, too (Konrad *et al.*, 2011; Michard *et al.*, 2017). PTs exhibit steep $[\text{Ca}^{2+}]_{\text{cyt}}$ and $[\text{H}^+]_{\text{cyt}}$ gradients, with a focused peak of concentration at the tip (Pierson *et al.*, 1994; Feijó *et al.*, 1999). Whereas some mechanistic links of $[\text{Ca}^{2+}]_{\text{cyt}}$ -regulation in PT growth are established, the role of pH-signaling is however unclear. Yet, the often occurring oscillatory PT growth behavior has been explored to characterize links between growth, $[\text{Ca}^{2+}]_{\text{cyt}}$ and extracellular H^+ fluxes (Damineli *et al.*, 2017). More recently, the demonstration that disruption of the pH gradient abrogates PT growth is suggestive of its critical role (Hoffmann *et al.*, 2020).

Live-cell imaging became an essential tool to visualize $[\text{Ca}^{2+}]_{\text{cyt}}$ and $[\text{H}^+]_{\text{cyt}}$ dynamics, monitoring signaling mechanisms and reporting on real-time ion transport (Uslu & Grossmann, 2016; Behera *et al.*, 2018; Grossmann *et al.*, 2018; Hilleary *et al.*, 2018; Walia *et al.*, 2018). The genetically encoded Ca^{2+} -sensors called GECOs (Zhao *et al.*, 2011), yield a fluorescence signal with a superior dynamic range compared to the ratiometric Ca^{2+} -sensor Yellow Cameleon 3.6 (YC3.6) (Keinath *et al.*, 2015). However, the drawback of the single-wavelength GECO-probes is that they are not ratiometric. Thus, spatial variations in protein abundance may reflect $[\text{Ca}^{2+}]_{\text{cyt}}$ dynamics inappropriately. This difficulty can be overcome by co-expression of a reference fluorescent protein for normalization (Waadt *et al.*, 2017). With exceptions (Ast *et al.*, 2017; Demes *et al.*, 2020; Waadt *et al.*, 2020), many of these methods do not warrant an equilibrated amount of the two

proteins to allow stable ratiometry free from unwanted FRET (Förster Resonance Energy Transfer). Close proximity of a reference and sensor fluorescent protein within a translational fusion protein carries the risk of FRET-effects to occur that may influence reporter readout, especially when the reference fluorescence protein is sensitive to cellular changes, too. This risk is particularly acute in the case of multiparametric monitoring. While recent advantages in Ca^{2+} -imaging highlight an interconnection of Ca^{2+} - and electric-signaling (Nguyen *et al.*, 2018) as well as Ca^{2+} - and pH-signaling (Behera *et al.*, 2018; Waadt *et al.*, 2020), the role for cytosolic pH-changes in plant physiology lags largely behind.

Here we set up a novel imaging technique and established an optimized biosensor we named 'CapHensor' enabling simultaneous ratiometric imaging of Ca^{2+} and pH, using two well-known genetically encoded probes arranged in a multicistronic vector harboring a P2A self-cleavage site. This arrangement allows spatial separation and equilibrated expression of the sensors from one messenger RNA (mRNA). We quantified coherency between cytosolic Ca^{2+} -, H^+ - and electric-signals and describe new interactions in ion signaling networks involved in the control of PT growth, stomata movement and leaf defense mechanisms.

Materials and Methods

Plant material, growth conditions and media

Growth of *Nicotiana tabacum* plants and pollen collection were performed as described (Gutermuth *et al.*, 2013). *Nicotiana benthamiana* was grown on soil under a 14 h : 10h, light : dark regime, at 26°C : 22°C in a glasshouse with *c.* 60% humidity.

The PT growth medium for experiments of Figs 1–3 was composed of: 1 mM 2-(*N*-morpholino)ethanesulfonic acid (MES), 0.2 mM calcium chloride (CaCl_2), 9.6 or 19.6 mM hydrochloric acid (HCl), and 1.6 mM boric acid (H_3BO_3). The pH of all solutions was adjusted to 5.8 with tris-(hydroxymethyl)-aminomethan (Tris) unless otherwise stated and osmolality adjusted to 420 mosmol kg^{-1} with D(+)-sucrose. *Nicotiana tabacum* GCs and *N. benthamiana* leaves were perfused with a standard solution for leaves (1 mM CaCl_2 , 1 mM potassium chloride (KCl) and 10 mM MES) adjusted to pH 5.8 with bis-tris propane (BTP). Either ABA (in 100% ethanol; Sigma-Aldrich, St Louis, MO, USA), hydrogen peroxide (H_2O_2) (Sigma-Aldrich), acetic acid (HAc; Applichem, Darmstadt, Germany), caffeine (Sigma-Aldrich), butyric acid (BTA) (Sigma-Aldrich) or flg22 (in water; Genscript, Piscataway, NJ, USA) was added to the solutions in the appropriate amounts and in case of pH changes, these were corrected with BTP.

Molecular biology, cloning and transformation

Cloning was performed with the USER cloning technique (Nour-Eldin *et al.*, 2006) and primers used are listed in Supporting Information Table S1. For stable transformation of *N. tabacum* plants or transient transformation of *N. benthamiana* leaves the *Agrobacterium tumefaciens* strain GV3101 was used.

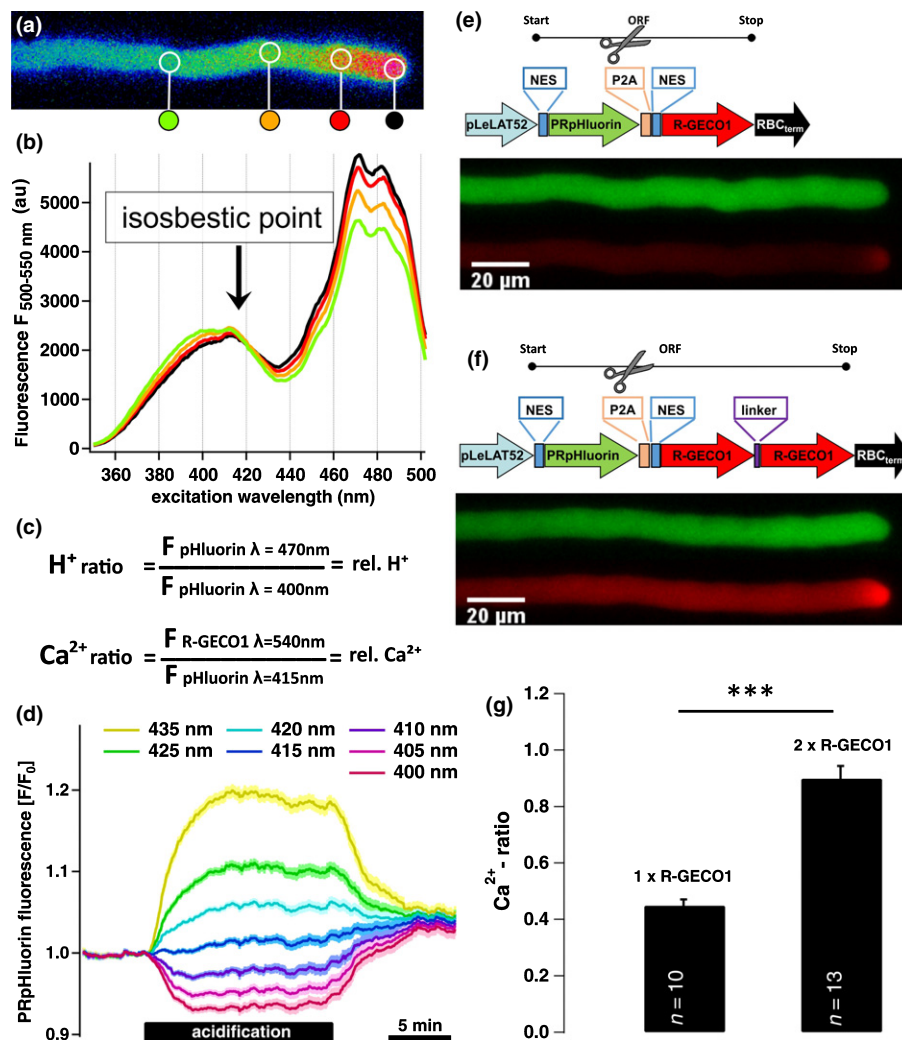


Fig. 1 Design, verification and functioning of CapHensor. The structure of the multicistronic CapHensor vectors and expression in PTs to verify its function. (a) False colored $[H^+]_{\text{cyt}}$ -ratio image of PRpHluorin transiently expressed in *Nicotiana tabacum* PTs. False color ranges from red, corresponding to slightly acidic lower pH (higher H^+ concentration) in the tip, to gradually dissipating green-blue values in the shank indicating moderate alkalization. (b) The marked circular regions-of-interest in (a) reflect the areas of extracting the PRpHluorin excitation spectra which are displayed with the same color. The intersection point of the excitation spectra (415 nm) represents the isosbestic point (marked by arrow), the point where there is no variation of emission at 525 ± 12.5 nm in response to pH. (c) Formulas to generate $[Ca^{2+}]_{\text{cyt}}$ and $[H^+]_{\text{cyt}}$ ratios to represent relative Ca^{2+} and H^+ concentrations, respectively. (d) Mean PRpHluorin fluorescence in mesophyll cells ($n = 67$) at the designated excitation wavelength after cellular acidification with 5 mM acetate (HAc). Despite progressive acidification, the fluorescence emission from the cytosol remains unchanged when excited with 415 nm. (e, f) Vector design and fluorescence intensity of PRpHluorin (green emission) and R-GECO1 (red emission) with the single or double R-GECO1 arrangement in stable transformed *N. tabacum* PTs. Spatial separation of the two fluorophores is achieved by the self-cleavage P2A sequence in the ORF indicated by the scissors. (g) Mean Ca^{2+} -ratio values from shank regions of PT expressing vector constructs shown in (e) and (f). The doubling of the ratio reflects the increase in the R-GECO1 emission when ratioed with the same emission generated by the PRpHluorin. Error bars = SE. The t -test was used in (g). ***, $P < 0.001$.

The LeLAT52 promotor (Twell *et al.*, 1991) and RBC-terminator or 35S promotor/terminator were used for PT or ubiquitous expression, respectively. Transient expression of PRpHluorin in PTs was performed as described (Gutermuth *et al.*, 2013).

The construct for cytosolic CapHensor targeting (pCambia3300 NES PRpHluorin NES P2A NES 2xR-GECO1) contained nuclear export sequences (NESs) at the N- and C-terminus of PRpHluorin as well as the N-terminus of the R-GECO1 tandem. The NES targeting sequences at the N- or C-terminus of PRpHluorin were from heat stable inhibitor (PKI) (Wen *et al.*, 1995; Matsushita *et al.*, 2003) and *Xenopus* MAPKK (Fukuda *et al.*, 1996),

respectively. The amino acid sequence of the linker between the two R-GECO1s was GLNLSGG, the 'self-cleaving' peptide P2A separating the coding sequence of PRpHluorin and R-GECO1 is as described (Kim *et al.*, 2011). Cytosolic expression of PRpHluorin in tobacco PT was possible with the N-terminal NES only. Nucleus localization was achieved by translational fusion of two nuclear localization sequences (NLSs) (pCambia3300 NLS NLS PRpHluorin P2A R-GECO1 NLS-linker R-GECO1) to the N-terminus of PRpHluorin and a NLS-linker between the two R-GECO1s originating from the simian virus 40 (SV40) T-antigen (Wen *et al.*, 1995; Krylova *et al.*, 2013).

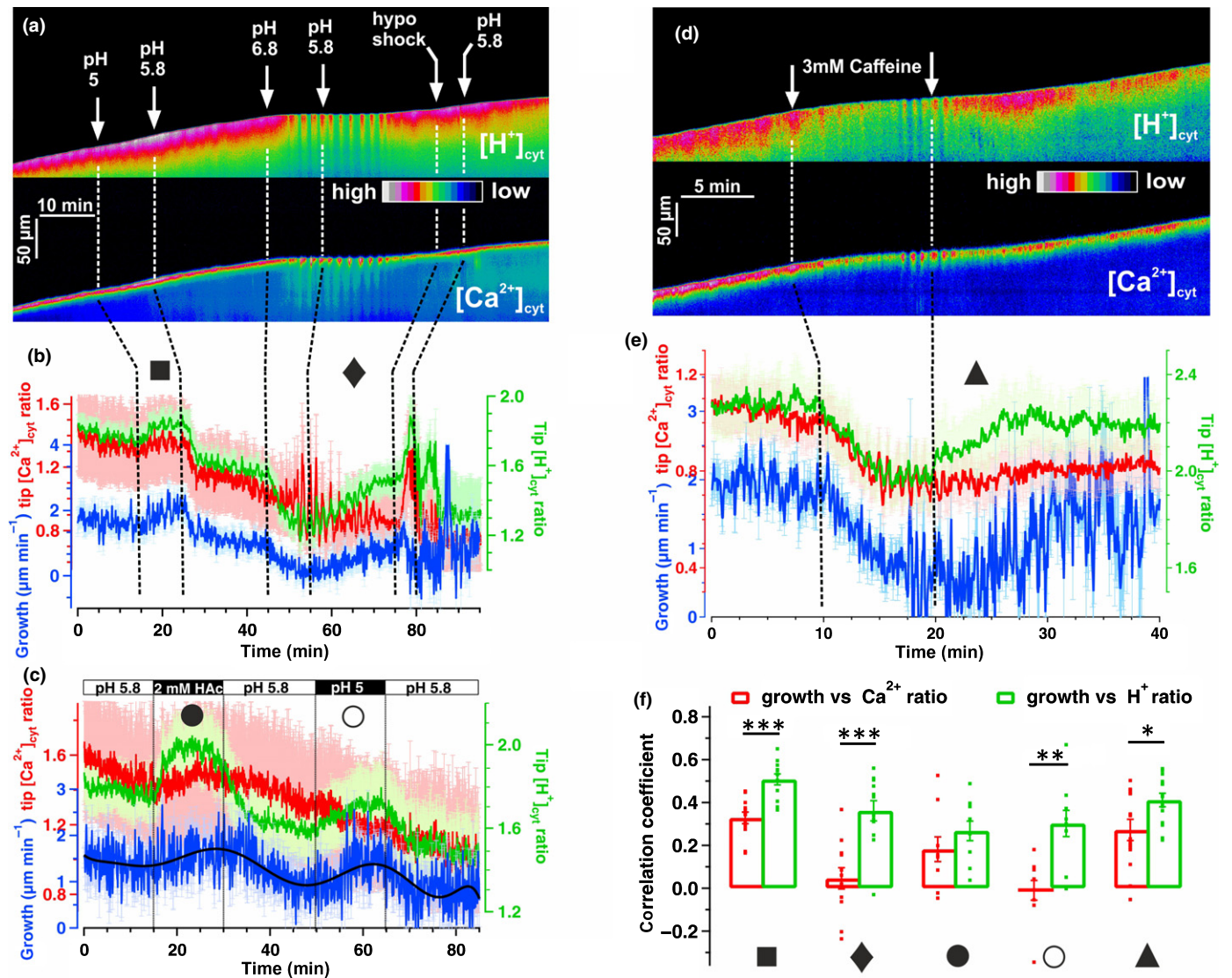


Fig. 2 Interrelation of $[Ca^{2+}]_{cyt}$, $[H^+]_{cyt}$ and growth in pollen tubes (PTs). Live-cell CapHensor imaging of *Nicotiana tabacum* PTs to quantify spatio-temporal interrelation of tip $[Ca^{2+}]_{cyt}$, $[H^+]_{cyt}$ and growth under different conditions. (a) False colored $[H^+]_{cyt}$ -ratio (top) and $[Ca^{2+}]_{cyt}$ -ratio (bottom) kymographs from a representative CapHensor PT imaging time-course experiment with sequential extracellular medium perfusions of different pH or low osmolarity (hypo shock). (b) Quantification of mean PT tip $[Ca^{2+}]_{cyt}$ (red line), $[H^+]_{cyt}$ (green line) and growth rate (blue line) from experiments ($n = 12$) with the same sequence of treatment as in (a). (c) Quantification of mean PT tip $[Ca^{2+}]_{cyt}$ (red line), $[H^+]_{cyt}$ (green line) and growth rate (blue line) from experiments ($n = 8$) upon 2 mM acetate (HAc) treatment or extracellular acidification (pH 5) in order to increase $[H^+]_{cyt}$. (d) False colored $[H^+]_{cyt}$ -ratio (top) and $[Ca^{2+}]_{cyt}$ -ratio (bottom) kymographs from a representative CapHensor PT imaging time-course experiment with sequential extracellular medium perfusion of 3 mM caffeine. (e) Quantification of mean PT tip $[Ca^{2+}]_{cyt}$ (red line), $[H^+]_{cyt}$ (green line) and growth rate (blue line) from experiments ($n = 15$) with the same sequence of treatment as in (d). (f) Comparison of correlation coefficients of growth vs tip $[Ca^{2+}]_{cyt}$ -ratio (red) and growth vs tip $[H^+]_{cyt}$ -ratio (green) from experiments in (b, ■ 15–25 min; ◆ 55–75 min), (c, ● 15–25 min; ○ 50–60 min) and (e, ▲ 20–30 min). Error bars = SE. Dots in (f) indicate individual measurements and *t*-test was used. *, $P < 0.05$; **, $P < 0.01$; ***, $P < 0.001$.

Expression in *Escherichia coli* and protein purification

R-GECO1 and 2×R-GECO1 in pET24 vector with an additional N-terminal StrepII-tag and YC3.6 in pET30a vector with an additional C-terminal StrepII-tag were introduced in *E. coli* BL21 (Stratagene, La Jolla, CA, USA). Proteins were expressed and purified as described (Guerra *et al.*, 2020). Great efforts were undertaken to remove Ca^{2+} -contaminations, as it is the main source of variations in quantifying half maximal effective concentration (EC_{50}) values from *in vitro* titration curves (Patton *et al.*,

2004). Briefly, 500 µl eluate was dialyzed using micro dialysis capsule QuixSep (Roth, Karlsruhe, Germany; 6000–8000-Da cutoff) against two buffer exchanges of 30 mM MES/Tris, 30 mM sodium chloride (NaCl), 5 mM EGTA (ethylene glycol-bis(β-aminoethyl ether)-*N,N,N,N*-tetraacetic acid) and against four buffer exchanges of 30 mM MES/Tris, 30 mM NaCl in ultra-quality water. To remove contaminating Ca^{2+} , plastic bottles, pipette tips, etc. were soaked in 5 mM EGTA and rinsed with ultra-quality water. All chemicals used were of the highest quality (> 99%; Roth, Karlsruhe, Germany).

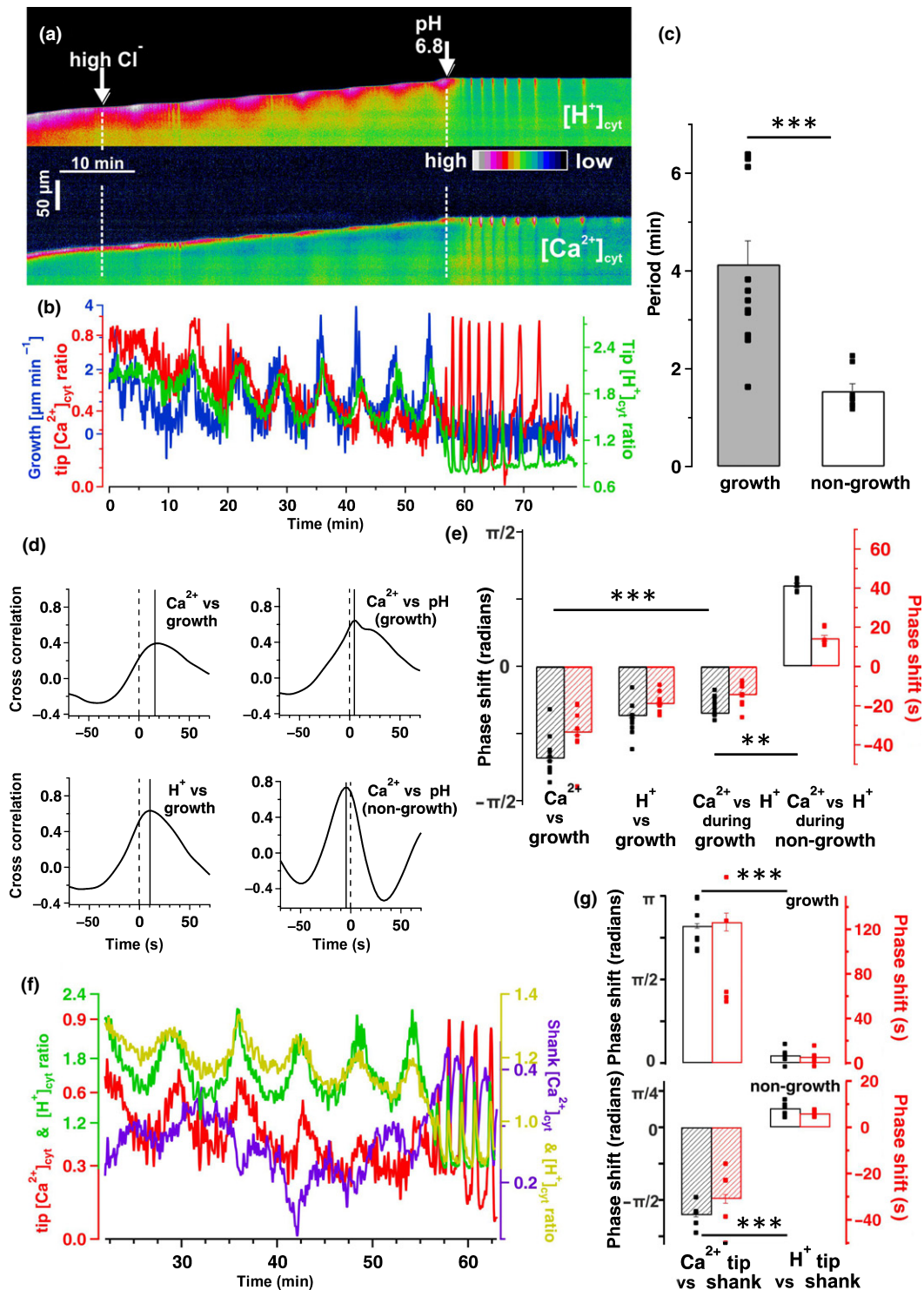


Fig. 3 Phase-relation analyses of [Ca²⁺]_{cyt}, [H⁺]_{cyt} and growth in oscillating pollen tubes (PTs). Live-cell CapHensor imaging of oscillating *Nicotiana tabacum* PTs to quantify spatio-temporal interrelation of ion signaling and growth. (a) False colored [H⁺]_{cyt}-ratio (top) and [Ca²⁺]_{cyt}-ratio (bottom) kymographs from a representative PT upon external challenging with 20 mM chloride (Cl⁻) and later challenged with both 20 mM Cl⁻ and pH 6.8 medium. (b) Quantification of PT tip [Ca²⁺]_{cyt} (red line), [H⁺]_{cyt} (green line) and growth rate (blue line) of the experiment in (a). (c) Mean period of [Ca²⁺]_{cyt}- and [H⁺]_{cyt}-ratio oscillations in growing (grey, n = 13) and non-growing (white, n = 8) PTs in high Cl⁻-solution. (d, e) Quantification of phase relationships via (d) cross-correlation and (e) cross-wavelet analyses from growing (n = 10) and non-growing (n = 8) PTs in high Cl⁻-solution as in (b). Time between the solid and dotted vertical lines corresponds to the lagging (shift to right side) or leading (shift to left side) signals in (d). Phase relationship of the signals is presented in radians (black) and also depicted as delay in seconds (red) in (e). (f) [Ca²⁺]_{cyt} and [H⁺]_{cyt} dynamics at the tip (left axis) and shank (right axis) from the cell in (a). (g) Quantification of phase relationships via cross-wavelet analyses between tip (1–5 μm from tip) and shank (35–40 μm from tip) from growing (upper bar diagram) and non-growing (lower bar diagram) PTs as exemplified in (f). It is important to note that delay times depicted in the correlation analyses in (d) and the wavelet analyses (e) are coherent despite being inverse. Error bars = SE. The *t*-test was used in (c) and (g) while one-way ANOVA was used in (e). **, *P* < 0.01; ***, *P* < 0.001.

In vitro biochemical characterization of Ca²⁺-sensors

For the analyses of Ca²⁺-sensor conformational changes high-Ca²⁺-buffer and zero-Ca²⁺-buffer (30 mM MES/Tris pH 7.35, 30 mM NaCl, 20 mM EGTA, \pm 20 mM CaCl₂) were mixed. Free Ca²⁺-concentrations were calculated with the WEBMXC extended website: <http://tinyurl.com/y48t33xq> based on Patton *et al.* (2004). To be able to compare the half maximal inhibitory concentration (IC₅₀) values of the three Ca²⁺-sensor constructs directly with each other, measurements were carried out with the same Ca²⁺ buffer solutions. Measurements were performed in a Tecan Spark with the following excitation (bandwidth 10 nm) and emission spectra (2 nm steps): R-GECO1 and 2×R-GECO1 (550 nm/584–660 nm), YC3.6 (435 nm/470–600 nm). For analyses of R-GECO1 and 2×R-GECO1 emission_{Max} from 586 to 600 nm was used, for YC3.6 we calculated the fluorescence ratio using maximal emission values of yellow fluorescent protein (YFP) (522–530 nm) over cyan fluorescent protein (CFP) (476–488 nm). Data was analyzed using Graphpad PRISM 5 (GraphPad Software Inc., La Jolla, CA, USA) and are described by a four parameter logistic equation. The best fit-value obtained for bottom and top ratio are used as F_{\min} and F_{\max} values to calculate the normalized fluorescence $F_{\text{norm}} = (F - F_{\min}) / (F_{\max} - F_{\min})$.

Live-cell- and confocal-imaging

Live-cell-imaging experiments were carried out with pollen or leaves of *N. tabacum* plants stably expressing the CapHensor versions. The microscope setup and imaging software is described in Gutermauth *et al.* (2013). For simultaneous Ca²⁺ and pH imaging in PTs, R-GECO1 and PRpHluorin were excited sequentially with the following order at 540, 400, 415 and 470 nm every 3 s. Intervals for CapHensor excitation in GCs and MCs were 5 and 3 s, respectively. A dual-band mirror (ET, Chroma 59001bs) was combined with a high-speed filter wheel equipped with bandpass filters for R-GECO (ET 605/26 nm) and PRpHluorin (ET 525/25 nm). To determine the isosbestic point, excitation wavelength was reflected by a LP 500 nm dichroic mirror combined with an ET 525/25 nm filter.

The procedure for pollen grain embedding, hardware and software for imaging is described in Gutermauth *et al.* (2013). For GC imaging epidermal strips were peeled from leaves of 5 to 6 weeks old tobacco plants and glued (with Medical Adhesive B, Ulrich Swiss, St Gallen, Switzerland) adaxial side down to cover slips mounted in custom made chambers. Epidermal peels recovered in standard solution for leaves for 3 to 6 h under a white light lamp (*c.* 20–25 $\mu\text{mol m}^{-2} \text{s}^{-1}$) at room temperature before the experiments. All experiments were carried out under permanent perfusion (700 $\mu\text{l min}^{-1}$). Stomatal movement was determined by means of quantifying the area within the stomatal pore in Fiji/IMAGEJ v.1.50 with a custom-made macro. For mesophyll imaging of *N. benthamiana* the abaxial epidermis of leaf discs was removed, while the adaxial side was glued to the cover slip with Medical Adhesive B followed by incubation in standard solution for leaves in darkness at room temperature for at least 12 h.

Confocal imaging was performed with a Leica TCS SP5 II equipped with a HCX IRAPO 25×/0.95 objective. PRpHluorin and R-GECO1 were excitation at 476 nm and 561 nm and fluorescence was captured at 530/30 nm and 617/26 nm, respectively. Chlorophyll fluorescence was captured at 680/37 nm. Image processing was performed with Fiji/IMAGEJ v.1.50. Data were processed and plotted with IGOR PRO 5.02 (Wavemetrics Inc., Portland, OR, USA) and R.

Quantification of Ca²⁺, pH, growth, membrane potential followed by coherence- and phase-relationship analyses

Guard cells (GCs) and mesophyll cells (MCs) Fluorescence intensity over time was extracted using Fiji/IMAGEJ followed by H⁺-ratio (PRpHluorin_{470nm}/PRpHluorin_{400nm}) and Ca²⁺ ratio (R-GECO1/PRpHluorin_{415nm}) calculations using the ‘image calculator’ tool. Subsequent phase analyses, correlation and wavelet transforms were performed with R v.3.6 (see later).

Pollen tubes (PTs) Quantification of growth, Ca²⁺- and H⁺-ratio were done as follows. Kymographs were generated using IMAGEJ (multiple kymograph plugin) and quantification of H⁺-ratio (PRpHluorin_{470nm}/PRpHluorin_{400nm}), Ca²⁺-ratio (R-GECO1/PRpHluorin_{415nm}), Ca²⁺ raw (R-GECO1) at the tip (1–5 μm behind the tip) and in the shank (35–40 μm behind the tip) was performed with R-scripts based on the CHUKNORRIS algorithm (Damineli *et al.*, 2017). Subsequent coherence analyses were performed.

Cross-wavelet and cross-correlation methodology for periodic phenomena in time series experiments was used to investigate correlation and coherence. Signals for Ca²⁺, H⁺, V_m and growth velocity were used to quantify their phase relationship with R-scripts called experiments_auto_analysis, phase_analysis, and CrossWaveGraph_pollen. A script called leaves_analysis was used to detect the time and value of the onset and peak response of Ca²⁺, H⁺ and stomata aperture area or V_m in GCs or MCs, respectively. All R-scripts, the CHUKNORRIS algorithm, and a set of example measurements including an instruction are compiled in Notes S1.

The wavelet transform was selected as the preferred method of analysis using the package WAVELETCOMP (Roesch & Schmidbauer, 2018) to estimate each signal as well as the coherent spectrum of each pair of signals (Ca²⁺-H⁺, Ca²⁺-growth, H⁺-growth, etc.). The dominant frequency of each signal over time was assessed which allows to define a phase relationship among them. The phase relationships reported are found on the ridges of the wavelet transformed and within the regions of statistical significance of the transformation as indicated by areas bordered by a white line in the wavelet spectra. Additionally, a running window correlation analysis of the signals (window size 50) was done allowing one to verify the relationship of the signals during the recordings.

Electrophysiology

Membrane voltage recordings with *N. benthamiana* leaves were carried out as described (Gutermauth *et al.*, 2013), but current-

clamp protocols were applied via WINEDR software (University of Strathclyde, Glasgow, UK). Electrode resistance was 60–120 M Ω .

Statistical analyses

Statistical analyses were carried out using GRAPHPAD software (GraphPad Software Inc.) and ORIGINPRO software (OriginLab, Northampton, MA, USA). Traces are demonstrated by means \pm standard errors (SEs). An unpaired *t*-test or one-way ANOVA was used to compare pairs of experimental conditions for statistically significant differences between groups (*, $P < 0.05$, **, $P < 0.01$; ***, $P < 0.001$).

Results

CapHensor design and functional validation

To monitor Ca^{2+} and pH in parallel we designed multicistronic vectors harboring two spectral distinct genetically encoded biosensors: PRpHluorin, based on the pH-dependent green fluorescent ratiometric pHluorin (Miesenböck *et al.*, 1998) which was optimized for plant usage (Shen *et al.*, 2013); and the red fluorescent Ca^{2+} -sensor R-GECO1 (Zhao *et al.*, 2011). These two well-characterized sensors were arranged within one original reading frame (ORF) harboring a self-cleavage P2A sequence (Kim *et al.*, 2011) resulting in posttranscriptional cleavage and a stoichiometric amount of both sensors. This dual-sensing approach was tested and verified in growing *N. tabacum* PTs, which was ideal because they sustain tip-focused $[\text{Ca}^{2+}]_{\text{cyt}}$ and $[\text{H}^+]_{\text{cyt}}$ gradients. The pH-dependent change in the excitation spectrum of PRpHluorin allows ratiometric imaging of the $[\text{H}^+]_{\text{cyt}}$ gradient in PTs (Fig. 1a) by sequential dual-excitation at 400 nm and 470 nm (Fig. 1b,c). In order to perform simultaneous ratiometric Ca^{2+} -imaging with the single-wavelength R-GECO1 probe (excitation at 540 nm), we ratioed its fluorescence using the excitation isosbestic point of PRpHluorin, where fluorescence is essentially pH- and Ca^{2+} -independent. The isosbestic point of PRpHluorin *in planta* was screened in growing PTs by recording its excitation spectrum, and determined to be around 410–420 nm (Fig. 1b). To resolve the isosbestic point exactly and validate its pH-insensitivity *in planta*, we monitored PRpHluorin fluorescence at seven distinct excitation wavelengths around to the isosbestic point while imposing $[\text{H}^+]_{\text{cyt}}$ changes by acetate (HAc) perfusion (Fig. 1d). In *N. tabacum* PTs and GCs (Fig. S1) as well as in *N. benthamiana* MCs (Fig. 1d), excitation at 415 nm (isosbestic point) produced no acetate-induced changes in PRpHluorin fluorescence. However, PRpHluorin fluorescence reacted to acidification when excited at wavelengths deviating from 415 nm (Fig. 1b). We concluded that PRpHluorin fluorescence when excited at 415 nm is pH-independent, allowing the use of this wavelength to ratio R-GECO1 fluorescence and allow Ca^{2+} -ratio quantitative measures (Fig. 1c). We further assumed that ratiometric measures using different proteins should be optimized using this strategy given that expression of PRpHluorin and R-GECO1 from the same promoter should result in quasi-

equimolar production of both proteins after P2A self-cleavage (Fig. 1e,f). This design should also prevent possible FRET to occur between the two fluorophores, optimizing fluorescence analysis and interpretation on the basis of ratiometry. Yet, a limitation arose from the relative low quantum yield of R-GECO1 when compared to green fluorescent protein (GFP) or YFP (Cranfill *et al.*, 2016). We solved that limitation by introducing two R-GECO1 ORFs in tandem. PT comparison from stable tobacco lines revealed the tandem sensor version to be much more effective (Fig. 1e,f): roughly twice the fluorescence from the R-GECO1, and the same amount of fluorescence emanating from the isosbestic point of PRpHluorin resulted in doubling of the R-GECO1 ratio value (Fig. 1e–g). *In vitro* biochemical characterization revealed comparable Ca^{2+} affinities for R-GECO1 and 2 \times R-GECO1 with a EC_{50} for Ca^{2+} of ≈ 350 nM (Fig. S2) consistent with reported values (Zhao *et al.*, 2011; Akerboom *et al.*, 2013; Inoue *et al.*, 2015). The EC_{50} values were *c.* 2 \times as high with YC3.6 (Fig. S2), demonstrating the ability of high sensitivity and high resolution Ca^{2+} -ratio measurements with the 2 \times R-GECO1 approach. We named the best performing tandem R-GECO1 design CapHensor. The characterization of the CapHensor in PTs could demonstrate its functionality and that of the dual ratiometric imaging method.

The tip focused pH-gradient represents a major determinant for pollen tube growth control

Next, we challenged growing PTs with different treatments to quantify interconnections in $[\text{Ca}^{2+}]_{\text{cyt}}$, $[\text{H}^+]_{\text{cyt}}$ and growth. *In vitro* growing PTs exhibit high $[\text{Ca}^{2+}]_{\text{cyt}}$ and $[\text{H}^+]_{\text{cyt}}$ at the tip (see Fig. 1a,f) (Holdaway-Clarke *et al.*, 1997; Feijó *et al.*, 1999; Guterthuth *et al.*, 2013; Hoffmann *et al.*, 2020) and extracellular pH changes and hypoosmotic shock were used here to perturb these gradients (Fig. 2a). The dynamics of $[\text{Ca}^{2+}]_{\text{cyt}}$, $[\text{H}^+]_{\text{cyt}}$ and growth rate was extracted from PT time-lapse series (Video S1), plotted in false-colored kymographs (Fig. 2a,b), and quantitatively analyzed using the CHUKNORRIS suite of statistical tools for image and time-series analysis (Damineli *et al.*, 2017). Acidification of the optimal growth medium from pH 5.8 to pH 5.0 increased growth rate, tip $[\text{H}^+]_{\text{cyt}}$ and tip $[\text{Ca}^{2+}]_{\text{cyt}}$ (Fig. 2a,b; Video S1). Inversely, alkalinizing the extracellular medium to pH 6.8 stopped PT growth, dissipated the $[\text{H}^+]_{\text{cyt}}$ constitutive gradient and lead to pronounced tip-focused high-amplitude $[\text{Ca}^{2+}]_{\text{cyt}}$ and $[\text{H}^+]_{\text{cyt}}$ oscillations (Fig. 2a,b; Video S1). Oscillations ceased and growth resumed after moving back to optimal pH 5.8 growth medium (Fig. 2a,b). Hypoosmotic shock resulted in transiently accentuated $[\text{Ca}^{2+}]_{\text{cyt}}$ and $[\text{H}^+]_{\text{cyt}}$ gradient at the tip (Fig. 2a,b; Video S1). Accentuating or dissipating the tip-focused $[\text{H}^+]_{\text{cyt}}$ gradient by experimental manipulations was associated to low or high growth rates, respectively (Fig. 2a,b). To test whether elevated growth rates were due to extracellular, or otherwise caused by cytosolic acidification in the apex, we made use of a medium supplemented with 2 mM acetate (HAc) adjusted to pH 5.8. The protonated form of HAc, a weak acid, is able to permeate membranes, releasing H^+ inside and thereby acidifying the cytosol (Brummer *et al.*, 1984). Therefore, using HAc with the

control medium adjusted to pH 5.8 only the cytosol acidifies whereas using low pH medium (pH 5.0), the cell wall and cytosol become acidified, due to the higher H^+ influx in the PT tip (Fig. 2a–c). The exclusive acidification of the cytosol by HAC increased growth rates (Fig. 2c) which is suggestive of an important role of tip $[H^+]_{\text{cyt}}$ to function as a key signal in PT growth control. Cytosolic acidification induced by extracellular pH 5, and HAC was both accompanied by a slight increase in $[Ca^{2+}]_{\text{cyt}}$ (Fig. 2b,c). Employing 3 mM caffeine to diminish the $[Ca^{2+}]_{\text{cyt}}$ gradient (Holdaway-Clarke *et al.*, 1997; Diao *et al.*, 2018), we recognized this treatment to dissipate both, the apical $[Ca^{2+}]_{\text{cyt}}$ as well as the $[H^+]_{\text{cyt}}$ gradient and to abrogate growth ($n=8$, Fig. 2d,e; Video S2). Correlation coefficients were calculated to evaluate the coherence of growth with tip $[Ca^{2+}]_{\text{cyt}}$ or $[H^+]_{\text{cyt}}$ in selected time windows marked by symbols in Fig. 2(b–e). It was evident, that during re-establishment of growth upon caffeine washout (Fig. 2e, triangle $t=20\text{--}30$ min), but also during recovery after the forced growth stop (Fig. 2b, diamond $t=55\text{--}75$ min) or during growth spurt caused by pH changes (Fig. 2b, square $t=15\text{--}25$ min and Fig. 2c, closed circle $t=15\text{--}25$ min, open circle $t=50\text{--}60$ min), growth rate correlated significantly better with tip $[H^+]_{\text{cyt}}$ rather than tip $[Ca^{2+}]_{\text{cyt}}$ (Fig. 3f). Coherence between growth and tip $[H^+]_{\text{cyt}}$ is consistent with other studies (Winship *et al.*, 2017; Hoffmann *et al.*, 2020) showing a prominent role of the $[H^+]_{\text{cyt}}$ gradient for PT growth.

To analyze coherence between $[Ca^{2+}]_{\text{cyt}}$, $[H^+]_{\text{cyt}}$ and growth with a good temporal resolution, we explored ion dynamics behavior in oscillating PTs. We used wavelet transformation (Torrence & Compo, 1998) as it is advantageous over cross-correlation analysis because dynamics in period length and power can be resolved in time, whereas cross-correlation analysis lack temporal information (Damineli *et al.*, 2017). Growth rate oscillations were induced by increasing Cl^- -concentration in the medium according to Guterthuth *et al.* (2013) (Video S3). Kymographs and corresponding quantifications of the PTs growth rate, tip $[Ca^{2+}]_{\text{cyt}}$ and $[H^+]_{\text{cyt}}$ over time demonstrated the three parameters to be clearly linked (Fig. 3a,b). Phase relationships between oscillations of growth rate, tip $[Ca^{2+}]_{\text{cyt}}$ and $[H^+]_{\text{cyt}}$ were quantified via wavelet and cross-wavelet analyses for representative sequences (Fig. 3a,b) and displayed in terms of dynamics of oscillatory power and period in the $[Ca^{2+}]_{\text{cyt}}$ and $[H^+]_{\text{cyt}}$ wavelet spectra (Fig. S3). Interestingly, the period of $[Ca^{2+}]_{\text{cyt}}$ and $[H^+]_{\text{cyt}}$ oscillations was reduced to roughly one-third upon alkalization induced growth arrests (pH 6.8) (Fig. 3c). This experimental sequence (increase in chloride followed by alkalization) was further explored to characterize phase delay changes between growth, $[Ca^{2+}]_{\text{cyt}}$ and $[H^+]_{\text{cyt}}$ oscillations. To that purpose, phase shifts in the $[Ca^{2+}]_{\text{cyt}}$ and $[H^+]_{\text{cyt}}$ oscillations were also converted into radians ($-\pi$; π) because it normalizes changes in period length allowing for better comparison of phase relations between measurements, and even between species (Holdaway-Clarke & Hepler, 2003). Quantification of the phase shifts between oscillations in growing PTs with cross-correlation analyses ($n=10$) (Fig. 3d) and cross-wavelet analyses ($n=10$) (Fig. 3e) revealed similar phase-shifts with mean $[Ca^{2+}]_{\text{cyt}}$ periods lagging behind $[H^+]_{\text{cyt}}$ periods by 14.55 ± 0.60 s, while growth lead $[H^+]_{\text{cyt}}$ periods by 17.87 ± 0.46 s (Fig. 3e). Note that lagging

and leading terms are used here not to imply causation, but simply to denominate the smallest interval of time, or the best cross-correlation between the two variables within the whole period length. It should be noted, however, that there is a growth spurt first, followed by the change in the $[H^+]_{\text{cyt}}$ gradient and then the change in the $[Ca^{2+}]_{\text{cyt}}$ gradient (Fig. 3d,e). Remarkably, phase relationships between $[Ca^{2+}]_{\text{cyt}}$ and $[H^+]_{\text{cyt}}$ inverted when PT growth was arrested (Fig. 3d,e). Non-growing oscillating PTs exhibited $[Ca^{2+}]_{\text{cyt}}$ -leading $[H^+]_{\text{cyt}}$ dynamics by 14.36 ± 1.42 s when growth arrest was induced by alkalizing the medium pH to 6.8 (Fig. 3e), but also displayed this phase relation in other media as long as growth was compromised (Fig. S4). Another interesting observation was that oscillations in $[Ca^{2+}]_{\text{cyt}}$ at the tip (red trace; 1–5 μm behind tip) and the shank (purple trace; 35–40 μm behind tip) were almost in antiphase (with absolute phase shift in radians values higher than half π) to one-another albeit the amplitude of shank Ca^{2+} -oscillations is smaller (Fig. 3f,g). The delay of $[Ca^{2+}]_{\text{cyt}}$ between the tip and shank was 126.48 ± 7.96 s in growing cells and 30.96 ± 1.86 s in non-growing cells, which was consistent with the period difference between growth and non-growth conditions (Figs 3g, S3). By contrast, $[H^+]_{\text{cyt}}$ alterations at the tip (green trace) were in phase (with absolute phase shift in radians values lower than half π) with the ones in the shank (light green; Fig. 3f, g) and unaltered by the PT growth state.

Distinct $[Ca^{2+}]_{\text{cyt}}$ and $[H^+]_{\text{cyt}}$ regimes triggered by different stimuli have particular control over stomatal movement

Another classic model system for ion signaling are stomata. Biotic and abiotic stimuli may induce second messenger signals but the relationship between $[Ca^{2+}]_{\text{cyt}}$ and $[H^+]_{\text{cyt}}$ have not yet been decoded. Initially, we set up an approach for synchronized imaging and stomatal movement in *N. tabacum* epidermal peels to investigate possible interrelation in GC motion, $[Ca^{2+}]_{\text{cyt}}$ and $[H^+]_{\text{cyt}}$ dynamics. Unexpectedly, stable expression of the CapHensor with a NES at the N-terminus of PRpHluorin and 2 \times R-GECO1 (Fig. 1f) resulted in additional fluorescence of PRpHluorin in the nucleus, while R-GECO1 located to the cytosol as expected (Fig. S5), so we designed different constructs to correct for that in stable transgenic tobacco. Of special note is, that none of the transgenic tobacco lines expressing various CapHensor versions had any negative effect on plant growth or reproduction (Fig. S6). Ideal for expression in leaves was a construct design harboring a second NES inserted at the C-terminus of PRpHluorin, resulting in exclusive cytosolic localization (Fig. S5) and fulfilling our criteria to optimize ratiometric imaging of $[Ca^{2+}]_{\text{cyt}}$ and $[H^+]_{\text{cyt}}$ (Fig. 4a).

In average, the application of 10 μM ABA ((\pm)-*cis,trans* ABA) to the pre-opened stomata induced a rapid $[H^+]_{\text{cyt}}$ decrease (alkalization) within 32.78 ± 6.13 s and an increase in $[Ca^{2+}]_{\text{cyt}}$ 80 ± 15.70 s after treatment, followed by stomatal closure (Fig. 4a,b; Video S4). Peak alkalization occurred at 190 ± 18.63 s and $[Ca^{2+}]_{\text{cyt}}$ peaked at 302.22 ± 13.47 s after ABA application, demonstrating the pH-response to occur before the $[Ca^{2+}]_{\text{cyt}}$ -change (Fig. 4c). We then investigated pathogen-induced stomatal closure induced by flg22, which despite inducing a similar

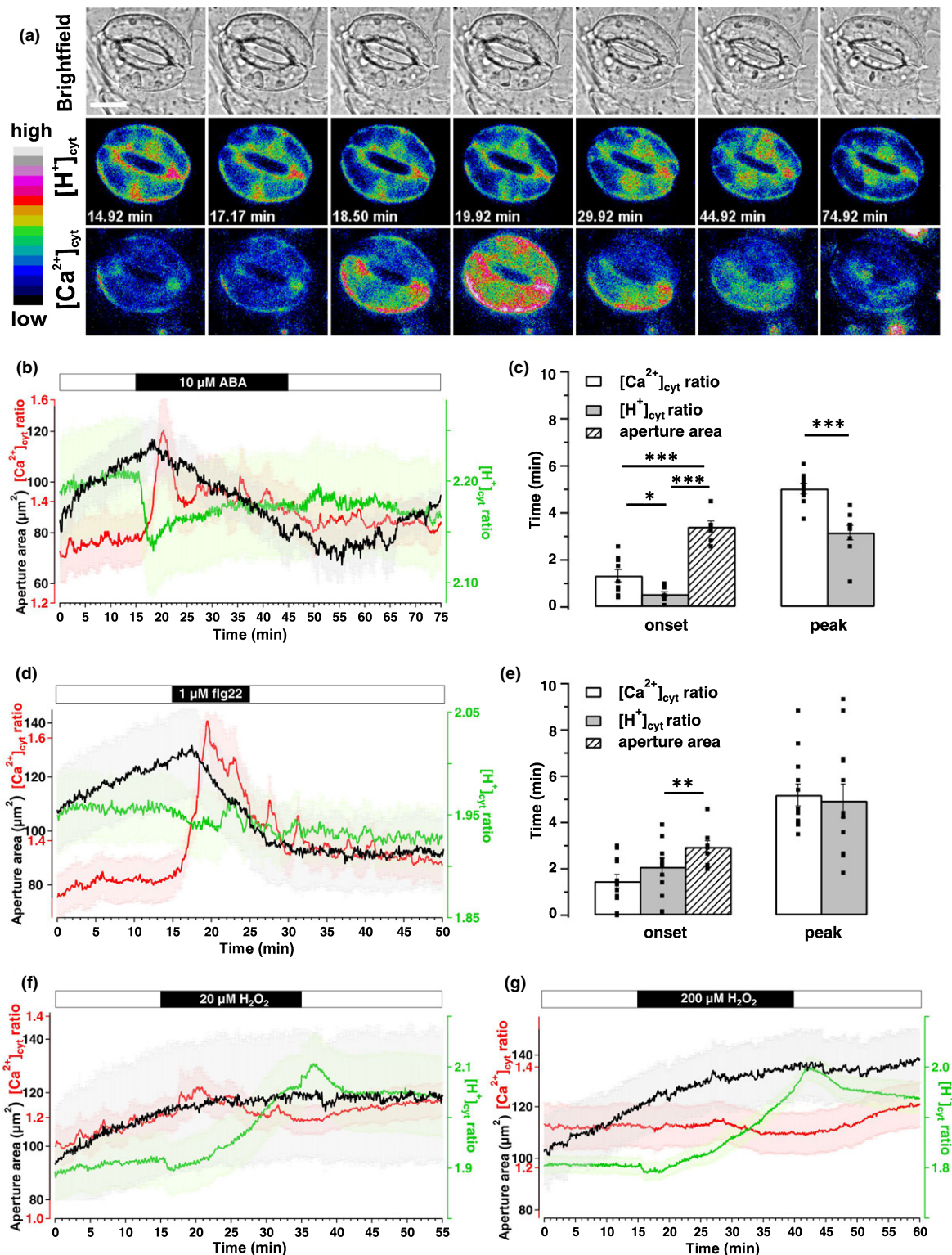


Fig. 4 Different stimuli trigger distinct $[Ca^{2+}]_{\text{cyt}}$ and $[H^+]_{\text{cyt}}$ signatures in guard cells (GCs) during stomata movement. Time-lapse CapHensor imaging together with stomata aperture monitoring in GCs of *Nicotiana tabacum* epidermal strips. (a) Brightfield (top) as well as false colored $[H^+]_{\text{cyt}}$ (middle) and $[Ca^{2+}]_{\text{cyt}}$ (bottom) ratio images of a representative time-lapse CapHensor imaging series upon the application of 10 μM ABA. Bar, 20 μm . (b, d, f, g) Mean $[Ca^{2+}]_{\text{cyt}}$ ratio (red), $[H^+]_{\text{cyt}}$ ratio (green) and stomatal aperture area (black) over time upon application of (b) 10 μM ABA ($n = 10$), (d) 1 μM flg22 ($n = 12$), (f) 20 μM H_2O_2 ($n = 10$) and (g) 200 μM H_2O_2 ($n = 22$). The bars above the mean traces indicate the time of treatments. (c, e) Bar diagram displays the average time of the onset and to the peak-response after 10 μM ABA and 1 μM flg22 treatment from data shown in (b) and (d), respectively. Dots in (c) and (e) indicate individual measurements. Error bars = SE. The t -test was used for peak time analyses while one-way ANOVA was used for onset time analyses in (c) and (e). *, $P < 0.05$; **, $P < 0.01$; ***, $P < 0.001$.

stomatal closure as ABA, induced no significant change in $[H^+]_{\text{cyt}}$. Surprisingly though, $[Ca^{2+}]_{\text{cyt}}$ response was more pronounced and lasted longer ($n=12$, Fig. 4d,e; Video S5). During stomatal closure induced by ABA and flg22 repetitive and sometimes oscillating spikes of $[Ca^{2+}]_{\text{cyt}}$ -increases occurred as previously described (Staxen *et al.*, 1999; Thor & Peiter, 2014) side-by-side with $[H^+]_{\text{cyt}}$ -oscillations (Fig. S7). Besides Ca^{2+} , ROS are widely considered important second messengers in ABA- and pathogen-signaling of GCs (Song *et al.*, 2014; Sierla *et al.*, 2016). For example, H_2O_2 at concentrations of 0.1–1 mM affect $[Ca^{2+}]_{\text{cyt}}$ -dynamics and in turn stomatal aperture (Pei *et al.*, 2000; Zhang *et al.*, 2001; Ma *et al.*, 2013; Martí *et al.*, 2013; Wu *et al.*, 2020). Surprisingly, application of 1 mM H_2O_2 resulted in loss of GC integrity in parallel with $[Ca^{2+}]_{\text{cyt}}$ and $[H^+]_{\text{cyt}}$ increases (Fig. S8; Video S6), but 20 and 200 μM H_2O_2 resulted in strong cytosol acidification within 10–20 min, while $[Ca^{2+}]_{\text{cyt}}$ and stomatal aperture were unaltered (Fig. 4f,g; Video S6).

All these results are suggestive of different signaling pathways to affect differently $[Ca^{2+}]_{\text{cyt}}$ and $[H^+]_{\text{cyt}}$, and thus we examined in more detail their possible correlation. Stomatal closure can be prevented by pH-clamping with the weak acid butyrate (Islam *et al.*, 2010; Ma *et al.*, 2013). Indeed, we could inhibit ABA-induced stomatal closure by perfusion with 10 μM ABA together with 3 mM BTA and as expected, BTA induced a moderate acidification (Fig. 5a) (*c.* 0.4 pH units according to the Henderson–Hasselbalch equation (Colcombet *et al.*, 2005)). In all cases, washing BTA while upholding 10 μM ABA caused an immediate drop in $[H^+]_{\text{cyt}}$ (alkalization), an increase in $[Ca^{2+}]_{\text{cyt}}$ and stomatal closure (Fig. 5a) ($n=22$). Intriguingly, ABA pre-incubated closed stomata opened immediately when an ABA-medium containing 3 mM BTA was applied (Fig. 5b). Similar to the BTA-inhibition of ABA-responses, 3 mM BTA inhibited flg22 induced stomata closure, however, pronounced $[Ca^{2+}]_{\text{cyt}}$ -increases occurred upon flg22-treatment in the presence of BTA ($n=24$, Fig. 5c). This suggests that $[Ca^{2+}]_{\text{cyt}}$ cannot be solely responsible for stomatal closure *per se*, and (as can be seen in Fig. 4b,c) supports our findings that ABA and flg22 trigger partially different ion signaling pathways but share pH-dependent mechanisms to trigger stomatal closure. To understand the interconnection between $[Ca^{2+}]_{\text{cyt}}$ and $[H^+]_{\text{cyt}}$ signals we increased extracellular Ca^{2+} known to close stomata (Gilroy *et al.*, 1991). This led to GC deflating together with transient oscillatory cytosolic alkalinizations and $[Ca^{2+}]_{\text{cyt}}$ increases ($n=22$, Figs 5d, S7) which is suggestive for control of stomata closure by alkalization and the existence of functional links between $[Ca^{2+}]_{\text{cyt}}$ and $[H^+]_{\text{cyt}}$.

Cytosolic and nuclear Ca^{2+} - and pH-changes are linked to electric signals in the mesophyll

Leaf mesophyll react to various stress stimuli with changes in $[Ca^{2+}]_{\text{cyt}}$, $[H^+]_{\text{cyt}}$ and V_m , and functional links between them have been suggested (Gilroy *et al.*, 2016). Hence, we carried out V_m recordings via sharp microelectrodes together with $[Ca^{2+}]_{\text{cyt}}$ / $[H^+]_{\text{cyt}}$ imaging in transiently transformed *N. benthamiana* leaves. Great care was taken to ensure that electrode insertion was close (next or above) to the imaging section. In contrast to the flg22

response in GCs (Fig. 4d), CapHensor expression in the cytosol of MCs (Fig. 6a) revealed pronounced $[H^+]_{\text{cyt}}$ and $[Ca^{2+}]_{\text{cyt}}$ increase upon 100 nM flg22 (Fig. 6b; Video S7). Interestingly, in all cases ($n=9$), flg22-induced a depolarization 125.72 ± 15.68 s after the given stimulus in the mesophyll (Fig. 6k, down 54 mV from a resting V_m of -114 ± 6.84 mV) that significantly preceded the $[Ca^{2+}]_{\text{cyt}}$ and $[H^+]_{\text{cyt}}$ changes by 121.61 ± 22.04 and 145.12 ± 20.13 s, respectively (Fig. 6b,i). However, the application of ABA and 200 μM H_2O_2 to MCs had no obvious chemo-electric response (Fig. 6c,d) and was comparable to control measurements (Fig. S9). It is well-known that pathogen attack (flg22) and drought stress (ABA) are transduced by H_2O_2 , leading to genetic reprogramming (Boudsocq *et al.*, 2010; Tsuda & Somssich, 2015; Couto & Zipfel, 2016; Li *et al.*, 2016; Birkenbihl *et al.*, 2017). Increases in nuclear Ca^{2+} concentrations ($[Ca^{2+}]_{\text{nuc}}$) play key roles in stress signaling pathways and induce changes in gene expression via CDPK-mediated and CaM-binding transcription factors (Reddy *et al.*, 2011; Dubiella *et al.*, 2013; Gao *et al.*, 2013). Based on the correlations between $[Ca^{2+}]_{\text{cyt}}$ and $[H^+]_{\text{cyt}}$ in PTs, GCs and MCs, we investigated their existence in the nucleus by generating a nuclear CapHensor version (Figs 6e, S9) to report $[Ca^{2+}]_{\text{nuc}}$ and nuclear H^+ concentrations ($[H^+]_{\text{nuc}}$). Similar to the chemo-electric response in the cytosol, $[Ca^{2+}]_{\text{nuc}}$ and $[H^+]_{\text{nuc}}$ transiently increased upon 100 nM flg22 (Fig. 6f,j; Video S7). The mean $[Ca^{2+}]_{\text{nuc}}$ and $[H^+]_{\text{nuc}}$ changes lagged behind the onset of the voltage changes of about 141.01 ± 22.09 and 117.51 ± 17.15 s, respectively, while the onset of $[Ca^{2+}]_{\text{nuc}}$ and $[H^+]_{\text{nuc}}$ approximately coincide at 226.29 ± 16.94 and 202.79 ± 12.59 s after treatment (Fig. 6j). This indicates that changes in concentration of both Ca^{2+} and H^+ in the cytosol induce similar changes in nuclear Ca^{2+} and H^+ . By contrast, application of ABA and 200 μM H_2O_2 to MCs revealed no obvious responses in V_m , $[Ca^{2+}]_{\text{nuc}}$ and $[H^+]_{\text{nuc}}$ (Fig. 6g,h).

Discussion

CapHensor advantages for high-resolution spatio-temporal imaging of Ca^{2+} and pH

Here we developed CapHensor a sophisticated dual reporter for simultaneous ratiometric imaging of Ca^{2+} and pH. Our design is based on multicistronic vectors for co-expression of an optimized pH-dependent GFP for plants and a red-fluorescent Ca^{2+} -sensor with a high dynamic range (Fig. 1). Our design circumvented, with advantage, other commonly observed problems with methods tailored for the same objectives (e.g. Waadt *et al.*, 2020), namely in terms of: (1) overcoming the low quantum yield of red fluorophores (Cranfill *et al.*, 2016); (2) increasing Ca^{2+} -sensitivity; (3) using the isosbestic point of PRpHluorin for Ca^{2+} -ratioing; (4) using of a self-cleavage P2A sequence to separate the two fluorophores; (5) allowing quantitative analysis free of variations in expression level and unwanted FRET events; (6) optimized subcellular targeting (Figs 1, 6, S5) avoiding problems with mixed signals from more than one compartment, a problem especially acute when considering different cytosolic and nuclear Ca^{2+} dynamics (Hanson & Köhler, 2001; Bootman *et al.*, 2009;

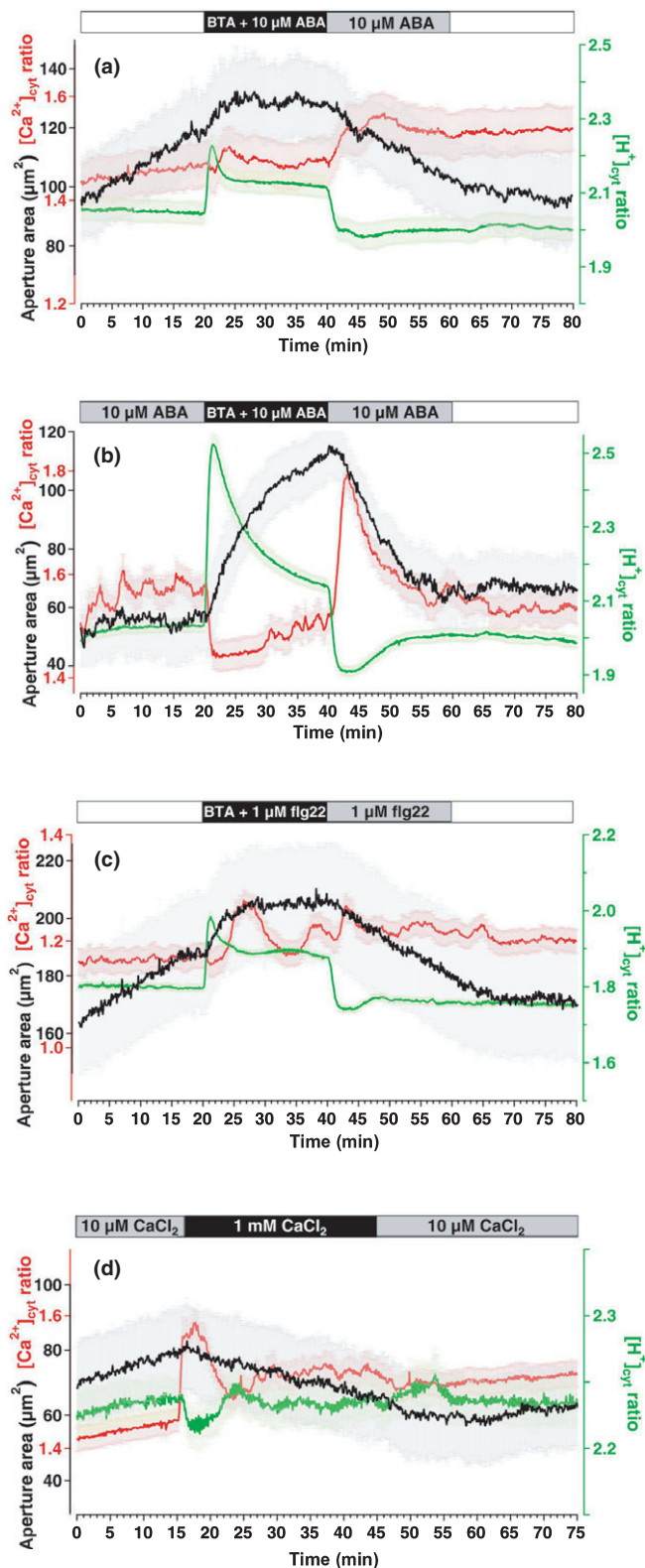


Fig. 5 The cytosolic pH in guard cells (GCs) – important factor for stoma movement. Time-lapse CapHensor imaging in GCs of *Nicotiana tabacum* epidermal strips together with stomata aperture monitoring. Mean $[Ca^{2+}]_{cyt}$ ratio (red), $[H^+]_{cyt}$ ratio (green) and stomata aperture area (black) over time. (a) Simultaneous application of 3 mM BTA and 10 μ M ABA followed by exclusive ABA treatment ($n = 22$). (b) 10 μ M ABA-pretreated GCs were challenged with 3 mM BTA plus 10 μ M ABA followed by treatment with 10 μ M ABA only ($n = 22$). (c) Simultaneous application of 3 mM BTA together with 1 μ M flg22 followed by exclusive flg22 treatment ($n = 24$). (d) Increase of the medium Ca^{2+} -concentration via perfusion from 10 μ M $CaCl_2$ to 1 mM $CaCl_2$ ($n = 22$) and back. Error bars = SE.

no such pH-effects on R-GECO1 fluorescence were observed upon triggering acidification in live PTs (Fig. 2c) or GCs (Fig. 5a–c). Moreover, no such visible pH effect on R-GECO1 fluorescence was observed during pronounced pH oscillations in PTs, GCs and MCs with different $[Ca^{2+}]_{cyt}$ - and $[H^+]_{cyt}$ phase relations (Figs 3e,g, 5a–d, 6b,f).

It should be noted that many conventional confocal laser microscopes lack a 415 nm laser line, the wavelength to excite PRpHluorin at its isosbestic point (Fig. 1). This does not allow Ca^{2+} -ratio measurements, that we achieved using a polychromator, or which is possible with a light-emitting diode-based system for illumination, however, CapHensor enables simultaneous monitoring of Ca^{2+} intensimetrically ($\Delta F/F_0$) and pH ratiometrically (405 nm laser diode and 476 nm argon laser line) with all advantages of its design.

Importance of the tip $[H^+]_{cyt}$ gradient in the signaling network of pollen tubes

Recently H^+ -ATPases were genetically established as the basis for the formation of the $[H^+]_{cyt}$ -gradient in PTs, with consequences on growth rates and plant fertility (Hoffmann *et al.*, 2020). In accordance, we generated here more evidence supporting an important role of the tip $[H^+]_{cyt}$ -gradient in PT growth regulation. CapHensor enabled visualizing decreased or increased growth rates when low or high tip $[H^+]_{cyt}$ was triggered on demand, respectively (Fig. 2a–f). This important relationship fits to the correlation coefficients between growth and $[H^+]_{cyt}$, which were significantly higher than those between growth and $[Ca^{2+}]_{cyt}$ (Fig. 2f). Detailed quantifications of phase relationships in oscillatory growing tobacco PTs showed the tip $[H^+]_{cyt}$ transients to precede the ones of tip $[Ca^{2+}]_{cyt}$ by *c.* 15 s, albeit $[H^+]_{cyt}$ transients still lagged growth by *c.* 18 s (Fig. 3b,e). In lily PTs a similar sequence of events was observed by Winship *et al.* (2017). The large phase shift between $[Ca^{2+}]_{cyt}$ and growth by *c.* 34 s, together with a lack of coherence between them (Fig. 2f) makes it difficult to argue for a causal relationship of Ca^{2+} inducing growth, though the involvement of Ca^{2+} channels in PT growth is well established. Our present data asks for a re-analysis of what the Ca^{2+} dependency of the mechanism behind PT growth might be.

Recently, it has been postulated, based on measurements on roots and leaves of *Arabidopsis*, that $[Ca^{2+}]_{cyt}$ increases lead to acidification of the cytosol (Behera *et al.*, 2018). PT oscillations however displayed phase relationships of $[Ca^{2+}]_{cyt}$ lagging $[H^+]_{cyt}$, that could be swapped during growth arrests, pointing to

Mazars *et al.*, 2011; Huang *et al.*, 2017; Charpentier, 2018; Kelnner *et al.*, 2018).

The pH-sensitivity of R-GECO1 *in planta* has been reported (Keinath *et al.*, 2015) and affects R-GECO1 fluorescence positively with alkalization (Zhao *et al.*, 2011). In our experiments

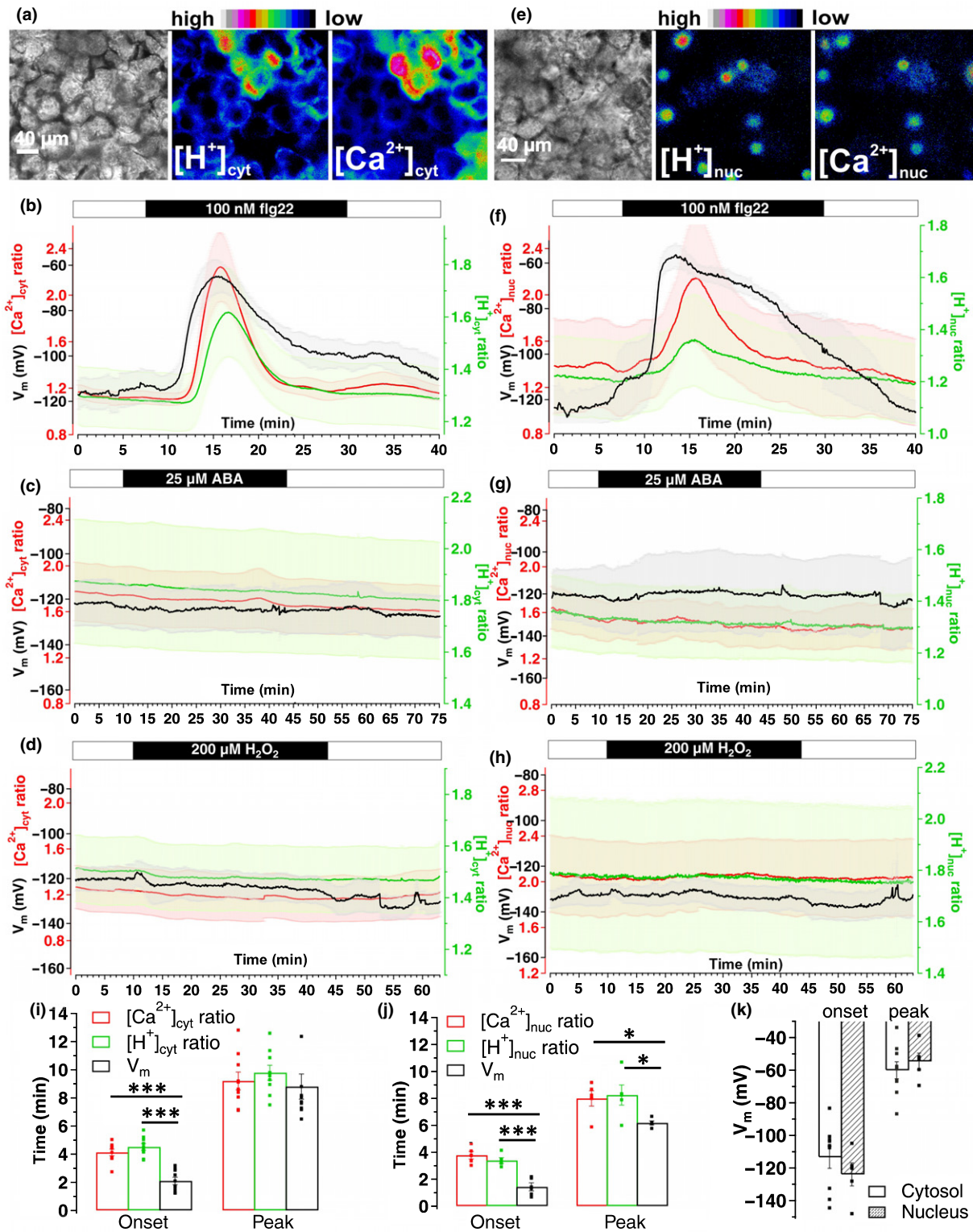


Fig. 6 Distinct cytosolic and nuclear Ca^{2+} - and H^+ -signatures in mesophyll cells upon different stimuli. Simultaneous Ca^{2+} , H^+ and V_m recordings in mesophyll cells of *Nicotiana benthamiana* leaves transiently expressing a cytosolic or nuclear version of the CapHensor. (a, e) Representative brightfield (left) as well as false colored $[\text{H}^+]$ - (middle) and $[\text{Ca}^{2+}]$ (right) ratio images of a leaf mesophyll section expressing the (a) cytosolic- or (e) nuclear CapHensor version. (b–d) Mean $[\text{Ca}^{2+}]_{\text{cyt}}$ ratio (red), $[\text{H}^+]_{\text{cyt}}$ ratio (green) and membrane potential (V_m , black) dynamics over time upon application of (b) 100 nM flg22 ($n = 9$), (c) 25 μM ABA ($n = 6$) and (d) 200 μM H_2O_2 ($n = 5$). (f–h) Mean $[\text{Ca}^{2+}]_{\text{nuc}}$ ratio (red), $[\text{H}^+]_{\text{nuc}}$ ratio (green) and V_m (black) dynamics over time upon application of (f) 100 nM flg22 ($n = 6$), (g) 25 μM ABA ($n = 4$) and (h) 200 μM H_2O_2 ($n = 5$). (i, j) Bar diagram of mean onset and peak times of Ca^{2+} ratio (red), H^+ ratio (green) and V_m after 100 nM flg22 with the cytosolic (i) or nuclear (j) expressed CapHensor. (k) Bar diagram of mean membrane potential (V_m) in mesophyll cells at the onset (left) and peak (right) response when the cytosol (blank, $n = 9$) or nucleus (shadow, $n = 6$) expressed version for CapHensor was used. Error bars = SE. Dots in (i–k) indicate individual measurements. One-way ANOVA was used in (i) and (j). *, $P < 0.05$; ***, $P < 0.001$.

a more dynamic interrelation of $[Ca^{2+}]_{\text{cyt}}$ and $[H^+]_{\text{cyt}}$ than previously thought. This has profound consequences for the understanding of a possible interdependence of these signaling ions and regulation of the corresponding transport proteins.

Another novel aspect revealed by CapHensor is the coupling of shank and tip oscillations, observed to be in antiphase for $[Ca^{2+}]_{\text{cyt}}$ while in phase for $[H^+]_{\text{cyt}}$ (Fig. 3f,g). Such delays may find an explanation on the physical properties of these ions and their interactions with organic molecules *in vivo*. On the one hand, the cytosol is presumed to have a high buffer capacity for Ca^{2+} and H^+ , but on the other hand, protons are predicted to have much higher diffusion rates (Vanýsek, 1993). Delays in shank vs tip could be viewed in the context of distinct subcellular locations and Ca^{2+} -affinities of CDPKs (Boudsocq *et al.*, 2012; Konrad *et al.*, 2018). Thus, it is conceivable that Ca^{2+} -regulated processes determining cell polarity like cytoskeleton dynamics (Cardenas *et al.*, 2008; Wang *et al.*, 2008; Hepler, 2016), organelle movement (Lovy-Wheeler *et al.*, 2007), and ion homeostasis (Tavares *et al.*, 2011; Zhao *et al.*, 2013; Gutermuth *et al.*, 2018) could be synchronized according to different temporal windows generated by the dynamics of these two ions.

Ca^{2+} and pH control stomata movement in concert – cytosolic pH affects ABA and pathogen signaling

Stomatal closure usually happens within 15 min after ABA application (McAinsh *et al.*, 1992; Staxen *et al.*, 1999; Tanaka *et al.*, 2005; Hubbard *et al.*, 2012). We posit that precise quantification of $[Ca^{2+}]_{\text{cyt}}$ and $[H^+]_{\text{cyt}}$ together with aperture monitoring, as we now describe, constitutes a new and relevant routine assay to ensure proper understanding of stomata signaling. In consonance, we demonstrate that $[Ca^{2+}]_{\text{cyt}}$ and $[H^+]_{\text{cyt}}$ are associated with different behaviors in GCs during ABA, flg22 and H_2O_2 responses. Stomatal closure by ABA depended on a rapid cytosolic alkalization, followed by $[Ca^{2+}]_{\text{cyt}}$ elevation (Figs 4, S7), preventing it blocked both stomatal closure and $[Ca^{2+}]_{\text{cyt}}$ elevations (Fig. 5a,b). The fact that closed stomata could be opened without delay by reversing the cytosolic alkalization even in the presence of ABA (Fig. 5a,b) is suggestive that the core ABA-signaling pathway is under pH-control. Such is the case of a key regulator in ABA-signaling, ABI1, where pH changes like those evoked by ABA were shown to modulate its activity (Leube *et al.*, 1998). ABI1 is one of the central regulators in ABA-signaling as it interacts with ABA receptors, SnRKs, CBL-CIPK and anion channels. This example could make the case for the presence of pH-sensing effector candidate proteins to exist and act in sensing pH signatures. The impact of such mechanisms could be far-reaching given that relevant roles for pH signaling, such as protons acting as *bona fide* neuro-transmitters (Beg *et al.*, 2008) have been proposed before. The fact that $[H^+]_{\text{cyt}}$ changes in GCs occur earlier than $[Ca^{2+}]_{\text{cyt}}$ changes and that the relationship between them is not fixed (Figs 4, 5, S7, S8) indicates a more complex interrelation between $[Ca^{2+}]_{\text{cyt}}$ and $[H^+]_{\text{cyt}}$ than previously thought (Behera *et al.*, 2018).

In contrast to the pH-dependent ABA-signaling pathway, the flg22-induced stomatal response mostly relies on a pronounced

$[Ca^{2+}]_{\text{cyt}}$ -increase as the $[H^+]_{\text{cyt}}$ dynamics was basically unchanged (Fig. 4d). This is in line with forward genetic screens that identified CDPKs and ROS production to be involved in flg22-dependent defense mechanisms (Boudsocq *et al.*, 2010). However, a quadruple loss-of-function mutant (CPK3/5/6/11) containing those CDPKs found in the screen was recently shown to have normal stomata behavior to ABA and flg22 (Güzel Deger *et al.*, 2015). This is suggestive of other Ca^{2+} -sensing or Ca^{2+} -independent mechanisms to be in place, as we could also block flg22-induced stomata closure by cytosolic acidification (Fig. 5c).

ABA- and flg22-induced stomata closure are believed to affect the production of ROS (Chinchilla *et al.*, 2007; Song *et al.*, 2014; Kimura *et al.*, 2017; Qi *et al.*, 2017), which were proposed to trigger yet unknown Ca^{2+} -channels (Mori & Schroeder, 2004; Song *et al.*, 2014). NADPH oxidases (RboHD/F) produce the major bulk of ROS required for flg22-induced stomatal closure, but not essential for ABA-induced stomatal closure (Toum *et al.*, 2016). In contrast to other studies in Arabidopsis (Allen *et al.*, 2000; Kwak *et al.*, 2003; Suhita *et al.*, 2004; Zou *et al.*, 2015; Wu *et al.*, 2020), $\leq 200 \mu\text{M}$ H_2O_2 treatment hardly closed tobacco stomata and increased $[Ca^{2+}]_{\text{cyt}}$ modestly, if at all (Fig. 4f,g). Slow stomata closure and a $[Ca^{2+}]_{\text{cyt}}$ rise was only observed with very high H_2O_2 concentrations (1 mM) where cell integrity was lost during a time-course of *c.* 15–30 min (Figs 4f,g, S8). It should be noted that H_2O_2 is known to be unspecific in terms of mimicking ABA-responses in terms of gene-expression (Trouverie *et al.*, 2008) and GC ion channel adjustment (Köhler *et al.*, 2003). However, we found physiological H_2O_2 concentrations to provoke a concentration-dependent, reversible and pronounced cytosolic acidification (Fig. 4f,g). Compatible with our results of a H_2O_2 -induced $[H^+]_{\text{cyt}}$ increase and a block of the ABA- and flg22-induced stomatal closure response by high $[H^+]_{\text{cyt}}$ in tobacco (Figs 4f,g, 5a–c), physiological concentrations of H_2O_2 were recently reported to open stomata in Arabidopsis (Li *et al.*, 2020).

Interconnection of Ca^{2+} -, pH- and electric signals in the mesophyll

Compared to GCs, MC physiology and its regulation by chemical and electrical signals is less well characterized. The leaf mesophyll is known to react quickly to wounding, pathogen infection or drought stress, sometimes generating rapid chemoelectric and transcriptional changes (Boudsocq *et al.*, 2010; Jeworutzki *et al.*, 2010; Krol *et al.*, 2010; Mousavi *et al.*, 2013; Keinath *et al.*, 2015; Toyota *et al.*, 2018; Berens *et al.*, 2019). Here, we combined the CapHensor approach with electrophysiology in mesophyll and revealed a steep $[Ca^{2+}]_{\text{cyt}}$ increase 4 min after flg22 treatment, that preceded a $[H^+]_{\text{cyt}}$ increase (acidification) by *c.* 24 s (Fig. 6b,i). The $[H^+]_{\text{cyt}}$ increase is consistent with an alkalization of the apoplast (Gust *et al.*, 2007; Jeworutzki *et al.*, 2010) suggested to play a role in long-distance stress signaling (Felle *et al.*, 2005; Zimmermann *et al.*, 2009; Geilfus, 2017). Cytosolic acidification was proposed to be involved in triggering defense gene expression in tobacco (Mathieu *et al.*, 1996; Lalous *et al.*, 1998). Indeed, we observed $[Ca^{2+}]_{\text{nuc}}$ and $[H^+]_{\text{nuc}}$ changes with

lower amplitude but similar timing in the nucleus upon flg22 treatment (Fig. 6f,j). Permeation of Ca^{2+} through nuclear pores is contentious, but the existence of Ca^{2+} -activated Ca^{2+} -channels in the nuclear envelope has been described (Kim *et al.*, 2019). Combining the improved features of CapHensor with electric recordings revealed novel aspects of the spatio-temporal relationships between V_m , $[\text{Ca}^{2+}]_{\text{cyt}}$ and $[\text{H}^+]_{\text{cyt}}$. Placing the electrode with the best possible precision was pivotal to monitor V_m and CapHensor fluorescence in the same area. It allowed the observation that large depolarizations start *c.* 2 min after flg22 application and precede $[\text{Ca}^{2+}]_{\text{cyt}}$ and $[\text{H}^+]_{\text{cyt}}$ increases by *c.* 2 min (Fig. 6b,f,i–k). This phenomenon was also recognized by others upon wounding (Zimmermann *et al.*, 2009) where V_m signals clearly travel faster than the accompanying $[\text{Ca}^{2+}]_{\text{cyt}}$ -waves (Nguyen *et al.*, 2018). Faster propagation of the depolarization signal when compared to the $[\text{Ca}^{2+}]_{\text{cyt}}$ -signal cannot be accounted for by a high cytosolic buffering capacity because diffusion of Ca^{2+} in cellular dimensions is accomplished in the millisecond to second range (Donahue & Abercrombie, 1987) and R-GECO1 is very sensitive to $[\text{Ca}^{2+}]_{\text{cyt}}$ -changes even close to the cells resting Ca^{2+} -level (Fig. S2). This questions the well-described mechanism of Ca^{2+} -dependent anion channel activation via CDPKs (Geiger *et al.*, 2011) to induce fast V_m changes seen here. The mesophyll depolarization was considered to be associated with anion efflux (Jeworutzki *et al.*, 2010), but post-translational modification of the H^+ -ATPase or its relocation into lipid domains may also contribute (Nühse *et al.*, 2007; Jeworutzki *et al.*, 2010; Keinath *et al.*, 2010). We thus have to conclude that the fast flg22-induced depolarization is neither mediated by Ca^{2+} nor H^+ or their signaling downstream effectors.

Analyses of V_m , Ca^{2+} and H^+ changes upon application of ABA and H_2O_2 resulted in no significant effects (Fig. 6c,d,g,h), showing that these do not induce fast cytosolic and/or nuclear signals in MCs. Hence, other Ca^{2+} and pH-independent mechanisms must exist. MCs and GCs thus seem to share signaling mechanisms for flg22, but not for ABA and H_2O_2 . Likewise, no responses to ABA and H_2O_2 on $[\text{Ca}^{2+}]_{\text{cyt}}$ and $[\text{H}^+]_{\text{cyt}}$ were recently reported in roots (Waadt *et al.*, 2020). We can therefore assume that GCs, PTs and MCs show different $[\text{Ca}^{2+}]_{\text{cyt}}/[\text{H}^+]_{\text{cyt}}$ interrelationships, which is consistent with the concept of distinct responses of different cell types (Harada & Shimazaki, 2008; Ranf *et al.*, 2011; Martí *et al.*, 2013). The relationship of Ca^{2+} -induced acidification in leaves and roots described recently (Behera *et al.*, 2018) is not apparent in every cell type as we presented for PTs and GCs here. In fact, Ca^{2+} /pH interrelations monitored via CapHensor displayed remarkable variability (Figs 3, 4, S7, S8). We conclude that when studying plant cellular signaling networks it is not possible to overgeneralize and draw conclusions from the response of one cell type to another.

Acknowledgements










The authors thank Robert Campbell and Gero Miesenböck for their permission to use R-GECO1 and pHluorin, respectively. The plant ratiometric pHluorin was kindly provided by Liwen Jiang. Early work on legacy versions of the CapHensor by Tilman

Güthoff is appreciated. The authors thank Bernadette Eichstädt for cloning of YC3.6 in the *E. coli* expression vector. For advice and discussion the authors are grateful to Dirk Becker. Financial support by the Deutsche Forschungsgemeinschaft (DFG KO3657/2-3) and Chinese Scholarship Council to Kai R. Konrad and Kunkun Li, respectively, is greatly acknowledged. The laboratory of JAF was supported by the National Institutes of Health (NIH, R01 GM131043) and the National Science Foundation (NSF, MCB1616437, MCB1637673 and MCB1930165). DSCD is funded by the grant 19/23343-7 from the São Paulo Research Foundation (FAPESP). For the use of the High Performance Computing Cluster the authors thank the ‘Rechenzentrum’ University of Würzburg. The authors would like to thank Marcel Dunkel (Visitron Systems) for providing the macro to measure excitation spectra with the VISIVIEW software.

Author contributions

KRK conceived and supervised the project, cloned legacy constructs, performed imaging, analyzed data, prepared figures and wrote the manuscript. KL performed most experiments, cloned, analyzed data and prepared figures. JP wrote R-scripts and performed analyses; DSCD developed a bespoke version of the CHUKNORRIS algorithm. AL performed biochemical work. TD, RH, TR and JAF edited and approved the final version of the manuscript.

ORCID

Daniel S. C. Damineli  <https://orcid.org/0000-0002-9911-2891>
 Thomas Dandekar  <https://orcid.org/0000-0003-1886-7625>
 José A. Feijó  <https://orcid.org/0000-0002-1100-5478>
 Rainer Hedrich  <https://orcid.org/0000-0003-3224-1362>
 Kai Robert Konrad  <https://orcid.org/0000-0003-4626-5429>
 Kunkun Li  <https://orcid.org/0000-0003-1597-197X>
 Anja Liese  <https://orcid.org/0000-0002-4766-2971>
 Juan Prada  <https://orcid.org/0000-0002-5214-7050>
 Tina Romeis  <https://orcid.org/0000-0002-0838-0031>

References

- Akerboom J, Carreras Calderón N, Tian L, Wabnig S, Prigge M, Toló J, Gordus A, Orger M, Severi K, Macklin J *et al.* 2013. Genetically encoded calcium indicators for multi-color neural activity imaging and combination with optogenetics. *Frontiers in Molecular Neuroscience* 6: 2.
- Allen GJ, Chu SP, Schumacher K, Shimazaki CT, Vafeados D, Kemper A, Hawke SD, Tallman G, Tsien RY, Harper JF *et al.* 2000. Alteration of stimulus-specific guard cell calcium oscillations and stomatal closing in *Arabidopsis det3* mutant. *Science* 289: 2338–2342.
- Ast C, Foret J, Oltrogge LM, De Michele R, Kleist TJ, Ho C-H, Frommer WB. 2017. Ratiometric Matryoshka biosensors from a nested cassette of green- and orange-emitting fluorescent proteins. *Nature Communications* 8: 431.
- Beg AA, Ernstrom GG, Nix P, Davis MW, Jorgensen EM. 2008. Protons act as a transmitter for muscle contraction in *C. elegans*. *Cell* 132: 149–160.
- Behera S, Xu Z, Luoni L, Bonza MC, Doccia FG, De Michelis MI, Morris RJ, Schwarzländer M, Costa A. 2018. Cellular Ca^{2+} signals generate defined pH signatures in plants. *The Plant Cell* 30: 2704–2719.
- Berens ML, Wolinska KW, Spaepen S, Ziegler J, Nobori T, Nair A, Krüler V, Winkelmüller TM, Wang Y, Mine A *et al.* 2019. Balancing trade-offs between

- biotic and abiotic stress responses through leaf age-dependent variation in stress hormone cross-talk. *Proceedings of the National Academy of Sciences, USA* 116: 2364–2373.
- Birkenbihl RP, Kracher B, Roccaro M, Somssich IE. 2017. Induced genome-wide binding of three Arabidopsis WRKY transcription factors during early MAMP-triggered immunity. *The Plant Cell* 29: 20–38.
- Blatt MR, Armstrong F. 1993. K^+ channels of stomatal guard cells – abscisic acid evoked control of the outward rectifier mediated by cytoplasmic pH. *Planta* 191: 330–341.
- Bootman MD, Fearnley C, Smyrniak I, MacDonald F, Roderick HL. 2009. An update on nuclear calcium signalling. *Journal of Cell Science* 122: 2337–2350.
- Boudsocq M, Droillard M-J, Regad L, Laurière C. 2012. Characterization of Arabidopsis calcium-dependent protein kinases: activated or not by calcium? *Biochemical Journal* 447: 291–299.
- Boudsocq M, Sheen J. 2013. CDPKs in immune and stress signaling. *Trends in Plant Science* 18: 30–40.
- Boudsocq M, Willmann MR, McCormack M, Lee H, Shan L, He P, Bush J, Cheng S-H, Sheen J. 2010. Differential innate immune signalling via Ca^{2+} sensor protein kinases. *Nature* 464: 418.
- Brandt B, Munemasa S, Wang C, Nguyen D, Yong T, Yang PG, Poretsky E, Belknap TF, Waadt R, Aleman F *et al.* 2015. Calcium specificity signaling mechanisms in abscisic acid signal transduction in Arabidopsis guard cells. *eLife* 4: e03599.
- Brummer B, Felle H, Parish RW. 1984. Evidence that acid solutions induce plant cell elongation by acidifying the cytosol and stimulating the proton pump. *FEBS Letters* 174: 223–227.
- Cardenas L, Lovy-Wheeler A, Kunkel JG, Hepler PK. 2008. Pollen tube growth oscillations and intracellular calcium levels are reversibly modulated by actin polymerization. *Plant Physiology* 146: 1611–1621.
- Charpentier M. 2018. Calcium signals in the plant nucleus: origin and function. *Journal of Experimental Botany* 69: 4165–4173.
- Chen K, Li G-J, Bressan RA, Song C-P, Zhu J-K, Zhao Y. 2020. Abscisic acid dynamics, signaling, and functions in plants. *Journal of Integrative Plant Biology* 62: 25–54.
- Chinchilla D, Zipfel C, Robatzek S, Kemmerling B, Nürnberger T, Jones JDG, Felix G, Boller T. 2007. A flagellin-induced complex of the receptor FLS2 and BAK1 initiates plant defence. *Nature* 448: 497–500.
- Choi W-G, Miller G, Wallace I, Harper J, Mittler R, Gilroy S. 2017. Orchestrating rapid long-distance signaling in plants with Ca^{2+} , ROS and electrical signals. *The Plant Journal* 90: 698–707.
- Colcombet J, Lelievre F, Thomine S, Barbier-Brygoo H, Frachisse JM. 2005. Distinct pH regulation of slow and rapid anion channels at the plasma membrane of *Arabidopsis thaliana* hypocotyl cells. *Journal of Experimental Botany* 56: 1897–1903.
- Cousson A, Vavasseur A. 1998. Putative involvement of cytosolic Ca^{2+} and GTP-binding proteins in cyclic GMP-mediated induction of stomatal opening by auxin in *Commelina communis* L. *Planta* 206: 308–314.
- Couto D, Zipfel C. 2016. Regulation of pattern recognition receptor signalling in plants. *Nature Reviews Immunology* 16: 537–552.
- Cranfill PJ, Sell BR, Baird MA, Allen JR, Lavagnino Z, de Gruiter HM, Kremers G-J, Davidson MW, Ustione A, Piston DW. 2016. Quantitative assessment of fluorescent proteins. *Nature Methods* 13: 557–562.
- Damineli DSC, Portes MT, Feijó JA. 2017. Oscillatory signatures underlie growth regimes in Arabidopsis pollen tubes: computational methods to estimate tip location, periodicity, and synchronization in growing cells. *Journal of Experimental Botany* 68: 3267–3281.
- Demes E, Besse L, Cubero-Font P, Satiat-Jeuemaitre B, Thomine S, De Angeli A. 2020. Dynamic measurement of cytosolic pH and $[NO_3^-]$ uncovers the role of the vacuolar transporter AtCLCa in cytosolic pH homeostasis. *Proceedings of the National Academy of Sciences, USA* 117: 15343–15353.
- Devireddy AR, Zandalinas SI, Gómez-Cadenas A, Blumwald E, Mittler R. 2018. Coordinating the overall stomatal response of plants: rapid leaf-to-leaf communication during light stress. *Science Signaling* 11: eaam9514.
- Diao M, Qu X, Huang S. 2018. Calcium imaging in Arabidopsis pollen cells using G-CaMP5. *Journal of Integrative Plant Biology* 60: 897–906.
- Donahue BS, Abercrombie RF. 1987. Free diffusion coefficient of ionic calcium in cytoplasm. *Cell Calcium* 8: 437–448.
- Dubiella U, Seybold H, Durian G, Komander E, Lassig R, Witte C-P, Schulze WX, Romeis T. 2013. Calcium-dependent protein kinase/NADPH oxidase activation circuit is required for rapid defense signal propagation. *Proceedings of the National Academy of Sciences, USA* 110: 8744–8749.
- Elzenga JTM, Prins HBA, Van Volkenburgh E. 1995. Light-induced membrane potential changes of epidermal and mesophyll cells in growing leaves of *Pisum sativum*. *Planta* 197: 127–134.
- Elzenga JTM, Volkenburgh EV. 1997. Kinetics of Ca^{2+} - and ATP-dependent, voltage-controlled anion conductance in the plasma membrane of mesophyll cells of *Pisum sativum*. *Planta* 201: 415–423.
- Feijó JA, Sainhas J, Hackett GR, Kunkel JG, Hepler PK. 1999. Growing pollen tubes possess a constitutive alkaline band in the clear zone and a growth-dependent acidic tip. *Journal of Cell Biology* 144: 483–496.
- Felle HH, Herrmann A, Huckelhoven R, Kogel KH. 2005. Root-to-shoot signalling: apoplastic alkalization, a general stress response and defence factor in barley (*Hordeum vulgare*). *Protoplasma* 227: 17–24.
- Fukuda M, Gotoh I, Gotoh Y, Nishida E. 1996. Cytoplasmic localization of mitogen-activated protein kinase directed by its NH₂-terminal, leucine-rich short amino acid sequence, which acts as a nuclear export signal. *Journal of Biological Chemistry* 271: 20024–20028.
- Gao D, Knight MR, Trewavas AJ, Sattelmacher B, Plieth C. 2004. Self-reporting arabidopsis expressing pH and Ca^{2+} indicators unveil ion dynamics in the cytoplasm and in the apoplast under abiotic stress. *Plant Physiology* 134: 898–908.
- Gao X, Chen X, Lin W, Chen S, Lu D, Niu Y, Li L, Cheng C, McCormack M, Sheen J *et al.* 2013. Bifurcation of Arabidopsis NLR immune signaling via Ca^{2+} -dependent protein kinases. *PLoS Pathogens* 9: e1003127.
- Geiger D, Maierhofer T, Al-Rasheid KAS, Scherzer S, Mumm P, Liese A, Ache P, Wellmann C, Marten I, Grill E *et al.* 2011. Stomatal closure by fast abscisic acid signaling is mediated by the guard cell anion channel SLAH3 and the receptor RCAR1. *Science Signaling* 4: ra32.
- Geilfus C-M. 2017. The pH of the Apoplast: dynamic factor with functional impact under stress. *Molecular Plant* 10: 1371–1386.
- Gilroy S, Białasek M, Suzuki N, Górecka M, Devireddy AR, Karpiński S, Mittler R. 2016. ROS, calcium, and electric signals: key mediators of rapid systemic signaling in plants. *Plant Physiology* 171: 1606–1615.
- Gilroy S, Fricker MD, Read ND, Trewavas AJ. 1991. Role of calcium in signal transduction of *Commelina* guard cells. *The Plant Cell* 3: 333–344.
- Grossmann G, Krebs M, Maizel A, Stahl Y, Vermeer JEM, Ott T. 2018. Green light for quantitative live-cell imaging in plants. *Journal of Cell Science* 131: jcs209270.
- Guerra T, Schilling S, Hake K, Gorzalka K, Sylvester F-P, Conrads B, Westermann B, Romeis T. 2020. Calcium-dependent protein kinase 5 links calcium signaling with N-hydroxy-L-pipecolic acid- and SARD1-dependent immune memory in systemic acquired resistance. *New Phytologist* 225: 310–325.
- Gust AA, Biswas R, Lenz HD, Rauhut T, Ranf S, Kemmerling B, Götz F, Glawischnig E, Lee J, Felix G *et al.* 2007. Bacteria-derived peptidoglycans constitute pathogen-associated molecular patterns triggering innate immunity in Arabidopsis. *Journal of Biological Chemistry* 282: 32338–32348.
- Gutermuth T, Herbell S, Lassig R, Brosche M, Romeis T, Feijó JA, Hedrich R, Konrad KR. 2018. Tip-localized Ca^{2+} -permeable channels control pollen tube growth via kinase-dependent R- and S-type anion channel regulation. *New Phytologist* 218: 1089–1105.
- Gutermuth T, Lassig R, Portes M-T, Maierhofer T, Romeis T, Borst J-W, Hedrich R, Feijó JA, Konrad KR. 2013. Pollen tube growth regulation by free anions depends on the interaction between the anion channel SLAH3 and calcium-dependent protein kinases CPK2 and CPK20. *The Plant Cell Online* 25: 4525–4543.
- Güzel Deger A, Scherzer S, Nuhkat M, Kedzierska J, Kollist H, Brosché M, Unyayar S, Boudsocq M, Hedrich R, Roelfsema MRG. 2015. Guard cell SLAC1-type anion channels mediate flagellin-induced stomatal closure. *New Phytologist* 208: 162–173.
- Hanson MR, Köhler RH. 2001. GFP imaging: methodology and application to investigate cellular compartmentation in plants. *Journal of Experimental Botany* 52: 529–539.

- Harada A, Shimazaki K-i. 2008. Measurement of changes in Cytosolic Ca^{2+} in Arabidopsis guard cells and mesophyll cells in response to blue light. *Plant and Cell Physiology* 50: 360–373.
- Hepler PK. 2016. The cytoskeleton and its regulation by calcium and protons. *Plant Physiology* 170: 3–22.
- Hilleary R, Choi W-G, Kim S-H, Lim SD, Gilroy S. 2018. Sense and sensibility: the use of fluorescent protein-based genetically encoded biosensors in plants. *Current Opinion in Plant Biology* 46: 32–38.
- Hoffmann RD, Portes MT, Olsen LI, Damineli DSC, Hayashi M, Nunes CO, Pedersen JT, Lima PT, Campos C, Feijó JA *et al.* 2020. Plasma membrane H^{+} -ATPases sustain pollen tube growth and fertilization. *Nature Communications* 11: 2395.
- Holdaway-Clarke TL, Feijó JA, Hackett GR, Kunkel JG, Hepler PK. 1997. Pollen tube growth and the intracellular cytosolic calcium gradient oscillate in phase while extracellular calcium influx is delayed. *The Plant Cell* 9: 1999–2010.
- Holdaway-Clarke TL, Hepler PK. 2003. Control of pollen tube growth: role of ion gradients and fluxes. *New Phytologist* 159: 539–563.
- Huang F, Luo J, Ning T, Cao W, Jin X, Zhao H, Wang Y, Han S. 2017. Cytosolic and nucleosolic calcium signaling in response to osmotic and salt stresses are independent of each other in roots of Arabidopsis seedlings. *Frontiers in Plant Science* 8: 1648.
- Hubbard KE, Siegel RS, Valerio G, Brandt B, Schroeder JI. 2012. Abscisic acid and CO_2 signalling via calcium sensitivity priming in guard cells, new CDPK mutant phenotypes and a method for improved resolution of stomatal stimulus-response analyses. *Annals of Botany* 109: 5–17.
- Inoue M, Takeuchi A, Horigane S-i, Ohkura M, Gengyo-Ando K, Fujii H, Kamijo S, Takemoto-Kimura S, Kano M, Nakai J *et al.* 2015. Rational design of a high-affinity, fast, red calcium indicator R-CaMP2. *Nature Methods* 12: 64–70.
- Irving HR, Gehring CA, Parish RW. 1992. Changes in cytosolic pH and calcium of guard cells precede stomatal movements. *Proceedings of the National Academy of Sciences, USA* 89: 1790–1794.
- Islam MM, Hossain MA, Jannat R, Munemasa S, Nakamura Y, Mori IC, Murata Y. 2010. Cytosolic alkalization and cytosolic calcium oscillation in Arabidopsis guard cells response to ABA and MeJA. *Plant and Cell Physiology* 51: 1721–1730.
- Jeworutzki E, Roelfsema MRG, Anschütz U, Krol E, Elzenga JTM, Felix G, Boller T, Hedrich R, Becker D. 2010. Early signaling through the Arabidopsis pattern recognition receptors FLS2 and EFR involves Ca^{2+} -associated opening of plasma membrane anion channels. *The Plant Journal* 62: 367–378.
- Jezek M, Blatt MR. 2017. The membrane transport system of the guard cell and its integration for stomatal dynamics. *Plant Physiology* 174: 487–519.
- Kadota Y, Sklenar J, Derbyshire P, Stransfeld L, Asai S, Ntoukakis V, Jones Jonathan D, Shirasu K, Menke F, Jones A *et al.* 2014. Direct regulation of the NADPH OXIDASE RBOHD by the PRR-associated kinase BIK1 during plant immunity. *Molecular Cell* 54: 43–55.
- Keinath NF, Kierszniowska S, Lorek J, Bourdais G, Kessler SA, Shimosato-Asano H, Grossniklaus U, Schulze WX, Robatzek S, Panstruga R. 2010. PAMP (pathogen-associated molecular pattern)-induced changes in plasma membrane compartmentalization reveal novel components of plant immunity. *The Journal of Biological Chemistry* 285: 39140–39149.
- Keinath NF, Waadt R, Brugman R, Schroeder JI, Grossmann G, Schumacher K, Krebs M. 2015. Live cell imaging with R-GECO1 sheds light on *flg22*- and chitin-induced transient $[\text{Ca}^{2+}]_{\text{Cyt}}$ patterns in Arabidopsis. *Molecular Plant* 8: 1188–1200.
- Kelner A, Leitao N, Chabaud M, Charpentier M, de Carvalho-Niebel F. 2018. Dual color sensors for simultaneous analysis of calcium signal dynamics in the nuclear and cytoplasmic compartments of plant cells. *Frontiers in Plant Science* 9: 14.
- Kim JH, Lee S-R, Li L-H, Park H-J, Park J-H, Lee KY, Kim M-K, Shin BA, Choi S-Y. 2011. High cleavage efficiency of a 2A peptide derived from Porcine teschovirus-1 in human cell lines, zebrafish and mice. *PLoS ONE* 6: e18556.
- Kim S, Zeng W, Bernard S, Liao J, Venkateshwaran M, Ane J-M, Jiang Y. 2019. Ca^{2+} -regulated Ca^{2+} channels with an RCK gating ring control plant symbiotic associations. *Nature Communications* 10: 3703.
- Kimura S, Waszczak C, Hunter K, Wrzaczek M. 2017. Bound by fate: the role of reactive oxygen species in receptor-like kinase signaling. *The Plant Cell* 29: 638–654.
- Köhler B, Hills A, Blatt MR. 2003. Control of guard cell ion channels by hydrogen peroxide and abscisic acid indicates their action through alternate signaling pathways. *Plant Physiology* 131: 385–388.
- Kollist H, Nuhkat M, Roelfsema MRG. 2014. Closing gaps: linking elements that control stomatal movement. *New Phytologist* 203: 44–62.
- Konrad KR, Maierhofer T, Hedrich R. 2018. Spatio-temporal aspects of Ca^{2+} signalling: lessons from guard cells and pollen tubes. *Journal of Experimental Botany* 69: 4195–4214.
- Konrad KR, Wudick MM, Feijó JA. 2011. Calcium regulation of tip growth: new genes for old mechanisms. *Current Opinion in Plant Biology* 14: 721–730.
- Krol E, Mentzel T, Chinchilla D, Boller T, Felix G, Kemmerling B, Postel S, Arents M, Jeworutzki E, Al-Rasheid KA *et al.* 2010. Perception of the Arabidopsis danger signal peptide 1 involves the pattern recognition receptor AtPEPR1 and its close homologue AtPEPR2. *Journal of Biological Chemistry* 285: 13471–13479.
- Krylova I, Kumar RR, Kofoed EM, Schaufele F. 2013. A versatile, bar-coded nuclear marker/reporter for live cell fluorescent and multiplexed high content imaging. *PLoS ONE* 8: e63286.
- Kudla J, Batistic O, Hashimoto K. 2010. Calcium signals: the lead currency of plant information processing. *The Plant Cell* 22: 541–563.
- Kumari A, Chételat A, Nguyen CT, Farmer EE. 2019. Arabidopsis H^{+} -ATPase AHA1 controls slow wave potential duration and wound-response jasmonate pathway activation. *Proceedings of the National Academy of Sciences, USA* 116: 201907379.
- Kwak JM, Mori IC, Pei ZM, Leonhardt N, Torres MA, Dangl JL, Bloom RE, Bodde S, Jones JD, Schroeder JI. 2003. NADPH oxidase *AtrbohD* and *AtrbohF* genes function in ROS-dependent ABA signaling in Arabidopsis. *EMBO Journal* 22: 2623–2633.
- Lapous D, Mathieu Y, Guern J, Laurière C. 1998. Increase of defense gene transcripts by cytoplasmic acidification in tobacco cell suspensions. *Planta* 205: 452–458.
- Leube MP, Grill E, Amrhein N. 1998. ABI1 of Arabidopsis is a protein serine/threonine phosphatase highly regulated by the proton and magnesium ion concentration. *FEBS Letters* 424: 100–104.
- Li B, Meng X, Shan L, He P. 2016. Transcriptional regulation of pattern-triggered immunity in plants. *Cell Host & Microbe* 19: 641–650.
- Li J-G, Fan M, Hua W, Tian Y, Chen L-G, Sun Y, Bai M-Y. 2020. Brassinosteroid and hydrogen peroxide interdependently induce stomatal opening by promoting guard cell starch degradation. *The Plant Cell* 32: 984–999.
- Lovy-Wheeler A, Cardenas L, Kunkel JG, Hepler PK. 2007. Differential organelle movement on the actin cytoskeleton in lily pollen tubes. *Cell Motility and the Cytoskeleton* 64: 217–232.
- Ma Y, She X, Yang S. 2013. Cytosolic alkalization-mediated H_2O_2 and NO production are involved in darkness-induced stomatal closure in *Vicia faba*. *Canadian Journal of Plant Science* 93: 119–130, 112.
- Martí MC, Stancombe MA, Webb AAR. 2013. Cell- and stimulus type-specific intracellular free Ca^{2+} signals in Arabidopsis. *Plant Physiology* 163: 625–634.
- Mathieu Y, Lapous D, Thomine S, Laurière C, Guern J. 1996. Cytoplasmic acidification as an early phosphorylation-dependent response of tobacco cells to elicitors. *Planta* 199: 416–424.
- Matsushita T, Mochizuki N, Nagatani A. 2003. Dimers of the N-terminal domain of phytochrome B are functional in the nucleus. *Nature* 424: 571–574.
- Mazars C, Brière C, Bourque S, Thuleau P. 2011. Nuclear calcium signaling: an emerging topic in plants. *Biochimie* 93: 2068–2074.
- McAinsh MR, Brownlee C, Hetherington AM. 1992. Visualizing changes in cytosolic free Ca^{2+} during the response of stomatal guard cells to abscisic acid. *The Plant Cell* 4: 1113–1122.
- McLachlan DH, Kopischke M, Robatzek S. 2014. Gate control: guard cell regulation by microbial stress. *New Phytologist* 203: 1049–1063.
- Melotto M, Underwood W, Koczan J, Nomura K, He SY. 2006. Plant stomata function in innate immunity against bacterial invasion. *Cell* 126: 969–980.
- Merilo E, Laanemets K, Hu H, Xue S, Jakobson L, Tulva I, Gonzalez-Guzman M, Rodriguez PL, Schroeder JI, Brosché M *et al.* 2013. PYR/RCAR receptors

- contribute to ozone-, reduced air humidity-, darkness-, and CO₂-induced stomatal regulation. *Plant Physiology* 162: 1652–1668.
- Michard E, Simon AA, Tavares B, Wudick MM, Feijó JA. 2017. Signaling with ions: the keystone for apical cell growth and morphogenesis in pollen tubes. *Plant Physiology* 173: 91–111.
- Miesenböck G, De Angelis DA, Rothman JE. 1998. Visualizing secretion and synaptic transmission with pH-sensitive green fluorescent proteins. *Nature* 394: 192–195.
- Moeder W, Phan V, Yoshioka K. 2019. Ca²⁺ to the rescue – Ca²⁺ channels and signaling in plant immunity. *Plant Science* 279: 19–26.
- Montillet J-L, Leonhardt N, Mondy S, Tranchimand S, Rumeau D, Boudsocq M, Garcia AV, Douki T, Bigeard J, Laurière C *et al.* 2013. An abscisic acid-independent oxylipin pathway controls stomatal closure and immune defense in Arabidopsis. *PLoS Biology* 11: e1001513.
- Mori IC, Murata Y, Yang YZ, Munemasa S, Wang YF, Andreoli S, Tiriach H, Alonso JM, Harper JF, Ecker JR *et al.* 2006. CDPKs CPK6 and CPK3 function in ABA regulation of guard cell S-type anion- and Ca²⁺-permeable channels and stomatal closure. *PLoS Biology* 4: 1749–1762.
- Mori IC, Schroeder JI. 2004. Reactive oxygen species activation of plant Ca²⁺ channels. A signaling mechanism in polar growth, hormone transduction, stress signaling, and hypothetically mechanotransduction. *Plant Physiology* 135: 702–708.
- Mousavi SA, Chauvin A, Pascaud F, Kellenberger S, Farmer EE. 2013. Glutamate receptor-like genes mediate leaf-to-leaf wound signalling. *Nature* 500: 422–426.
- Murata Y, Mori IC, Munemasa S. 2015. Diverse stomatal signaling and the signal integration mechanism. *Annual Review of Plant Biology* 66: 369–392.
- Nguyen CT, Kurenda A, Stolz S, Chételat A, Farmer EE. 2018. Identification of cell populations necessary for leaf-to-leaf electrical signaling in a wounded plant. *Proceedings of the National Academy of Sciences, USA* 115: 10178–10183.
- Nour-Eldin HH, Hansen BG, Norholm MH, Jensen JK, Halkier BA. 2006. Advancing uracil-excision based cloning towards an ideal technique for cloning PCR fragments. *Nucleic Acids Research* 34: e122.
- Nühse TS, Bottrill AR, Jones AME, Peck SC. 2007. Quantitative phosphoproteomic analysis of plasma membrane proteins reveals regulatory mechanisms of plant innate immune responses. *The Plant Journal: For Cell and Molecular Biology* 51: 931–940.
- Patton C, Thompson S, Epel D. 2004. Some precautions in using chelators to buffer metals in biological solutions. *Cell Calcium* 35: 427–431.
- Pei ZM, Murata Y, Benning G, Thomine S, Klusener B, Allen GJ, Grill E, Schroeder JI. 2000. Calcium channels activated by hydrogen peroxide mediate abscisic acid signalling in guard cells. *Nature* 406: 731–734.
- Pierson ES, Miller DD, Callahan DA, Shipley AM, Rivers BA, Cresti M, Hepler PK. 1994. Pollen tube growth is coupled to the extracellular calcium ion flux and the intracellular calcium gradient: effect of BAPTA-type buffers and hypertonic media. *The Plant Cell Online* 6: 1815–1828.
- Qi J, Wang J, Gong Z, Zhou J-M. 2017. Apoplastic ROS signaling in plant immunity. *Current Opinion in Plant Biology* 38: 92–100.
- Ranf S, Eschen-Lippold L, Pecher P, Lee J, Scheel D. 2011. Interplay between calcium signalling and early signalling elements during defence responses to microbe- or damage-associated molecular patterns. *The Plant Journal* 68: 100–113.
- Reddy ASN, Ali GS, Celesnik H, Day IS. 2011. Coping with stresses: roles of calcium- and calcium/calmodulin-regulated gene expression. *The Plant Cell* 23: 2010–2032.
- Roelfsema MRG, Hedrich R, Geiger D. 2012. Anion channels: master switches of stress responses. *Trends in Plant Science* 17: 221–229.
- Roesch A, Schmidbauer H. 2018. *WaveletComp: computational wavelet analysis*. R package v. 1.1. [WWW document] URL <https://CRAN.R-project.org/package=WaveletComp>.
- Romeis T, Herde M. 2014. From local to global: CDPKs in systemic defense signalling upon microbial and herbivore attack. *Current Opinion in Plant Biology* 20: 1–10.
- Shen J, Zeng Y, Zhuang X, Sun L, Yao X, Pimpl P, Jiang L. 2013. Organelle pH in the Arabidopsis endomembrane system. *Molecular Plant* 6: 1419–1437.
- Sierla M, Waszczak C, Vahisalu T, Kangasjärvi J. 2016. Reactive oxygen species in the regulation of stomatal movements. *Plant Physiology* 171: 1569–1580.
- Song Y, Miao Y, Song C-P. 2014. Behind the scenes: the roles of reactive oxygen species in guard cells. *New Phytologist* 201: 1121–1140.
- Staxen II, Pical C, Montgomery LT, Gray JE, Hetherington AM, McAinsh MR. 1999. Abscisic acid induces oscillations in guard-cell cytosolic free calcium that involve phosphoinositide-specific phospholipase C. *Proceedings of the National Academy of Sciences, USA* 96: 1779–1784.
- Stoelzle S, Kagawa T, Wada M, Hedrich R, Dietrich P. 2003. Blue light activates calcium-permeable channels in Arabidopsis mesophyll cells via the phototropin signaling pathway. *Proceedings of the National Academy of Sciences, USA* 100: 1456–1461.
- Suhita D, Raghavendra AS, Kwak JM, Vavasseur A. 2004. Cytoplasmic alkalization precedes reactive oxygen species production during methyl jasmonate- and abscisic acid-induced stomatal closure. *Plant Physiology* 134: 1536–1545.
- Suzuki N, Miller G, Salazar C, Mondal HA, Shulaev E, Cortes DF, Shuman JL, Luo X, Shah J, Schlauch K *et al.* 2013. Temporal-spatial interaction between reactive oxygen species and abscisic acid regulates rapid systemic acclimation in plants. *The Plant Cell* 25: 3553–3569.
- Tanaka Y, Sano T, Tamaoki M, Nakajima N, Kondo N, Hasezawa S. 2005. Ethylene inhibits abscisic acid-induced stomatal closure in Arabidopsis. *Plant Physiology* 138: 2337–2343.
- Tavares B, Dias PN, Domingos P, Moura TF, Feijó JA, Bicho A. 2011. Calcium-regulated anion channels in the plasma membrane of *Lilium longiflorum* pollen protoplasts. *New Phytologist* 192: 45–60.
- Thor K, Peiter E. 2014. Cytosolic calcium signals elicited by the pathogen-associated molecular pattern flg22 in stomatal guard cells are of an oscillatory nature. *New Phytologist* 204: 873–881.
- Tian W, Hou C, Ren Z, Wang C, Zhao F, Dahlbeck D, Hu S, Zhang L, Niu Q, Li L *et al.* 2019. A calmodulin-gated calcium channel links pathogen patterns to plant immunity. *Nature* 572: 131–135.
- Torrence C, Compo GP. 1998. A practical guide to wavelet analysis. *Bulletin of the American Meteorological Society* 79: 61–78.
- Toum L, Torres PS, Gallego SM, Benavides MP, Vojnov AA, Gudesblat GE. 2016. Coronatine inhibits stomatal closure through guard cell-specific inhibition of NADPH oxidase-dependent ROS production. *Frontiers in Plant Science* 7: 1851.
- Toyota M, Spencer D, Sawai-Toyota S, Jiaqi W, Zhang T, Koo AJ, Howe GA, Gilroy S. 2018. Glutamate triggers long-distance, calcium-based plant defense signaling. *Science* 361: 1112–1115.
- Trouverie J, Vidal G, Zhang Z, Sirichandra C, Madiona K, Amiar Z, Prioul J-L, Jeannette E, Rona J-P, Brault M. 2008. Anion channel activation and proton pumping inhibition involved in the plasma membrane depolarization induced by ABA in *Arabidopsis thaliana* suspension cells are both ROS dependent. *Plant and Cell Physiology* 49: 1495–1507.
- Tsuda K, Somssich IE. 2015. Transcriptional networks in plant immunity. *New Phytologist* 206: 932–947.
- Twell D, Yamaguchi J, Wing RA, Ushiba J, McCormick S. 1991. Promoter analysis of genes that are coordinately expressed during pollen development reveals pollen-specific enhancer sequences and shared regulatory elements. *Genes & Development* 5: 496–507.
- Uslu VV, Grossmann G. 2016. The biosensor toolbox for plant developmental biology. *Current Opinion in Plant Biology* 29: 138–147.
- Vanýsek P. 1993. Ionic conductivity and diffusion at infinite dilution. In: Linde DR, ed. *CRC hand book of chemistry and physics, 74th edn*. Boca Raton, FL, USA: CRC Press, 5-90–5-92.
- Vincent TR, Avramova M, Canham J, Higgins P, Bilkey N, Mugford ST, Pitino M, Toyota M, Gilroy S, Miller AJ *et al.* 2017. Interplay of plasma membrane and vacuolar ion channels, together with BAK1, elicits rapid cytosolic calcium elevations in Arabidopsis during aphid feeding. *The Plant Cell* 29: 1460–1479.
- Waadt R, Koster P, Andres Z, Waadt C, Bradamante G, Lampou K, Kudla J, Schumacher K. 2020. Dual-reporting transcriptionally linked genetically encoded fluorescent indicators resolve the spatiotemporal coordination of cytosolic abscisic acid and second messenger dynamics in Arabidopsis. *The Plant Cell* 32: 2582–2601.

- Waadt R, Krebs M, Kudla J, Schumacher K. 2017. Multiparameter imaging of calcium and abscisic acid and high-resolution quantitative calcium measurements using R-GECO1-mTurquoise in Arabidopsis. *New Phytologist* 216: 303–320.
- Walia A, Waadt R, Jones AM. 2018. Genetically encoded biosensors in plants: pathways to discovery. *Annual Review of Plant Biology* 69: 497–524.
- Wang H-J, Wan A-R, Jauh G-Y. 2008. An actin-binding protein, LILIM1, mediates calcium and hydrogen regulation of actin dynamics in pollen tubes. *Plant Physiology* 147: 1619–1636.
- Wen W, Meinkotht JL, Tsien RY, Taylor SS. 1995. Identification of a signal for rapid export of proteins from the nucleus. *Cell* 82: 463–473.
- Wilkins KA, Matthus E, Swarbreck SM, Davies JM. 2016. Calcium-mediated abiotic stress signaling in roots. *Frontiers in Plant Science* 7: 1296.
- Winship LJ, Rounds C, Hepler PK. 2017. Perturbation analysis of calcium, alkalinity and secretion during growth of lily pollen tubes. *Plants* 6: 3.
- Wu F, Chi Y, Jiang Z, Xu Y, Xie L, Huang F, Wan D, Ni J, Yuan F, Wu X *et al.* 2020. Hydrogen peroxide sensor HPCA1 is an LRR receptor kinase in Arabidopsis. *Nature* 578: 577–581.
- Yan S, McLamore ES, Dong S, Gao H, Taguchi M, Wang N, Zhang T, Su X, Shen Y. 2015. The role of plasma membrane H⁺-ATPase in jasmonate-induced ion fluxes and stomatal closure in *Arabidopsis thaliana*. *The Plant Journal* 83: 638–649.
- Young JJ, Mehta S, Israelsson M, Godoski J, Grill E, Schroeder JI. 2006. CO₂ signaling in guard cells: calcium sensitivity response modulation, a Ca²⁺-independent phase, and CO₂ insensitivity of the *gca2* mutant. *Proceedings of the National Academy of Sciences, USA* 103: 7506–7511.
- Yuan P, Jauregui E, Du L, Tanaka K, Poovaiah BW. 2017. Calcium signatures and signaling events orchestrate plant–microbe interactions. *Current Opinion in Plant Biology* 38: 173–183.
- Zhang X, Dong FC, Gao JF, Song CP. 2001. Hydrogen peroxide-induced changes in intracellular pH of guard cells precede stomatal closure. *Cell Research* 11: 37–43.
- Zhao L-N, Shen L-K, Zhang W-Z, Zhang W, Wang Y, Wu W-H. 2013. Ca²⁺-dependent protein Kinase11 and 24 modulate the activity of the inward rectifying K⁺ channels in Arabidopsis pollen tubes. *The Plant Cell Online* 25: 649–661.
- Zhao Y, Araki S, Wu J, Teramoto T, Chang Y-F, Nakano M, Abdelfattah AS, Fujiwara M, Ishihara T, Nagai T *et al.* 2011. An expanded palette of genetically encoded Ca²⁺ indicators. *Science* 333: 1888–1891.
- Zheng X, Kang S, Jing Y, Ren Z, Li L, Zhou J-M, Berkowitz G, Shi J, Fu A, Lan W *et al.* 2018. Danger-associated peptides close stomata by OST1-independent activation of anion channels in guard cells. *The Plant Cell* 30: 1132–1146.
- Zimmermann MR, Maischak H, Mithöfer A, Boland W, Felle HH. 2009. System potentials, a novel electrical long-distance apoplastic signal in plants, induced by wounding. *Plant Physiology* 149: 1593–1600.
- Zou J-J, Li X-D, Ratnasekera D, Wang C, Liu W-X, Song L-F, Zhang W-Z, Wu W-H. 2015. Arabidopsis CALCIUM-DEPENDENT PROTEIN KINASE8 and CATALASE3 function in abscisic acid-mediated signaling and H₂O₂ homeostasis in stomatal guard cells under drought stress. *The Plant Cell* 27: 1445–1460.

Supporting Information

Additional Supporting Information may be found online in the Supporting Information section at the end of the article.

Fig. S1 Isosbestic point of PRpHluorin in pollen tubes and guard cells.

Fig. S2 Ca²⁺ binding to YC3.6 and R-GECO1 *in vitro*.

Fig. S3 [Ca²⁺]_{cyt} and [H⁺]_{cyt} oscillations period in pollen tube under high Cl⁻ solution.

Fig. S4 Pollen tube growth arrest is associated with tip [Ca²⁺]_{cyt} oscillations preceding [H⁺]_{cyt} oscillations, which is independent on the pH-gradient across the plasma membrane.

Fig. S5 Subcellular localization of CapHensor versions in guard cells.

Fig. S6 Transgenic *Nicotiana tabacum* CapHensor lines grow normal.

Fig. S7 [Ca²⁺]_{cyt} and [H⁺]_{cyt} oscillations in individual guard cells upon ABA, flg22 and high Ca²⁺ treatment.

Fig. S8 1 mM H₂O₂ results in loss of guard cell integrity.

Fig. S9 Ca²⁺, H⁺ and V_m regime in the mesophyll under control conditions.

Notes S1 R-scripts for quantitative analysis of data from pollen tubes, guard cells and mesophyll cells.

Table S1 Primers for cloning and sequencing of CapHensor constructs.

Video S1 Time-lapse CapHensor imaging of a representative *Nicotiana tabacum* PT from Fig. 2(a,b) with false colored [H⁺]_{cyt} and [Ca²⁺]_{cyt} ratios, and widefield image (bottom) upon sequential extracellular medium perfusions of different pH or low osmolarity (hypo shock).

Video S2 Time-lapse CapHensor imaging of a representative *Nicotiana tabacum* PT from Fig. 2(d,e) with false colored [H⁺]_{cyt} and [Ca²⁺]_{cyt} ratios, and widefield image upon 3 mM caffeine perfusion.

Video S3 Time-lapse CapHensor imaging of a representative *Nicotiana tabacum* PT from data presented in Fig. 3(a,b) with false colored [H⁺]_{cyt} and [Ca²⁺]_{cyt} ratios, and widefield image.

Video S4 Time-lapse CapHensor imaging of a representative *Nicotiana tabacum* GC in epidermal strip presented in Fig. 4(a) with false colored [H⁺]_{cyt} and [Ca²⁺]_{cyt} ratios, and widefield image.

Video S5 Time-lapse CapHensor imaging of a representative *Nicotiana tabacum* GC in epidermal strip presented in Fig. 4(d) with false colored [H⁺]_{cyt} and [Ca²⁺]_{cyt} ratios, and widefield image.

Video S6 Two time-lapse CapHensor imaging series of representative *Nicotiana tabacum* GCs in epidermal strips upon 200 μM H₂O₂ or 1 mM H₂O₂ treatment corresponding to data presented

in Figs 4(g) and S8 showing false colored $[H^+]_{\text{cyt}}$ and $[Ca^{2+}]_{\text{cyt}}$ ratios, as well as widefield images.

Video S7 Two time-lapse imaging series of $[H^+]$ - and $[Ca^{2+}]$ -ratio images as well as brightfield images from *Nicotiana benthamiana* mesophyll tissue responding to 0.1 μM flg22 when expressing the cytosolic or nuclear version of the CapHensor, corresponding to data presented in Fig. 6(b,f).

Please note: Wiley Blackwell are not responsible for the content or functionality of any Supporting Information supplied by the authors. Any queries (other than missing material) should be directed to the *New Phytologist* Central Office.



About *New Phytologist*

- *New Phytologist* is an electronic (online-only) journal owned by the New Phytologist Foundation, a **not-for-profit organization** dedicated to the promotion of plant science, facilitating projects from symposia to free access for our Tansley reviews and Tansley insights.
- Regular papers, Letters, Viewpoints, Research reviews, Rapid reports and both Modelling/Theory and Methods papers are encouraged. We are committed to rapid processing, from online submission through to publication 'as ready' via *Early View* – our average time to decision is <26 days. There are **no page or colour charges** and a PDF version will be provided for each article.
- The journal is available online at Wiley Online Library. Visit **www.newphytologist.com** to search the articles and register for table of contents email alerts.
- If you have any questions, do get in touch with Central Office (np-centraloffice@lancaster.ac.uk) or, if it is more convenient, our USA Office (np-usaoffice@lancaster.ac.uk)
- For submission instructions, subscription and all the latest information visit **www.newphytologist.com**